



HAL
open science

BHLS₂ and $\pi^+\pi^-$ Final State Interaction : The $\eta/\eta' \rightarrow \pi^+\pi^-\gamma$ Decays and the Muon HVP

M Benayoun, L Delbuono, F Jegerlehner

► **To cite this version:**

M Benayoun, L Delbuono, F Jegerlehner. BHLS₂ and $\pi^+\pi^-$ Final State Interaction : The $\eta/\eta' \rightarrow \pi^+\pi^-\gamma$ Decays and the Muon HVP. 2023. hal-04234677v2

HAL Id: hal-04234677

<https://hal.science/hal-04234677v2>

Preprint submitted on 10 Oct 2023 (v2), last revised 27 Mar 2024 (v3)

HAL is a multi-disciplinary open access archive for the deposit and dissemination of scientific research documents, whether they are published or not. The documents may come from teaching and research institutions in France or abroad, or from public or private research centers.

L'archive ouverte pluridisciplinaire **HAL**, est destinée au dépôt et à la diffusion de documents scientifiques de niveau recherche, publiés ou non, émanant des établissements d'enseignement et de recherche français ou étrangers, des laboratoires publics ou privés.

BHLS₂ and $\pi^+\pi^-$ Final State Interaction : The $\eta/\eta' \rightarrow \pi^+\pi^-\gamma$ Decays and the Muon HVP

M. Benayoun^{a†}, L. DelBuono^a, F. Jegerlehner^b

^a LPNHE des Universités Paris VI et Paris VII, IN2P3/CNRS, F-75252 Paris, France

^b Humboldt-Universität zu Berlin, Institut für Physik, Newtonstrasse 15, D-12489 Berlin, Germany

September 27, 2023

Abstract

The departure of the latest FNAL experimental average for the muon anomalous magnetic moment $a_\mu = (g_\mu - 2)/2$ measurements having increased from 4.2σ [1] to 5.0σ [2], with respect to the White Paper (WP) consensus[3], it may indicate a hint for new physics. As the most delicate piece of a_μ is its leading order HVP part a_μ^{HVP-LO} , methods to ascertain its theoretical value are crucial to interpret appropriately this departure with the measurement. We therefore propose to examine closely the dipion spectra from the $\eta/\eta' \rightarrow \pi^+\pi^-\gamma$ decays in the Hidden Local Symmetry (HLS) context using its BHLS₂ broken variant. We thus have at disposal a framework where the close relationship of the dipion spectra from the η/η' and τ decays and of the $e^+e^- \rightarrow \pi^+\pi^-$ annihilation can be simultaneously considered. A special focus is put to the high statistic dipion spectra from the η decay collected by the KLOE/KLOE2 Collaboration and η' decay collected by the BESIII Collaboration. It is shown that, once the Final State Interaction (FSI) effects are accounted for, the BHLS₂ framework provides a fair account of their dipion spectra. More precisely, it is first proven that a single FSI polynomial is requested, common to both the η and η' dipion spectra. Moreover, it is shown that fits involving the $\eta/\eta'/\tau$ dipion spectra, and excluding the $e^+e^- \rightarrow \pi^+\pi^-$ annihilation data, allow for a prediction of the pion form factor data $F_\pi(s)$ which fairly agree with the usual dipion spectra collected in the $e^+e^- \rightarrow \pi^+\pi^-$ annihilation channel. Even if more precise $\eta/\eta'/\tau$ dipion spectra would help to be fully conclusive, this may already be considered as supporting the Dispersive Approach results for a_μ^{HVP-LO} .

† *Maurice Benayoun has passed on September 15th, 2023.*

Contents

1	Preamble : Various Aspects of the Dispersive Approach to the Muon HVP	2
2	Introduction	5
3	The Kroll Conditions and VPP Lagrangian Pieces	7
4	The $\eta/\eta' \rightarrow \pi^- \pi^+ \gamma$ Decays in the BHLS₂ Framework	8
5	The $\eta \rightarrow \pi^+ \pi^- \gamma$ Amplitude within BHLS₂	9
6	The $\eta' \rightarrow \pi^+ \pi^- \gamma$ Amplitude within BHLS₂	11
7	BHLS₂ and the WZW Box Anomalies	12
8	η/η' Radiative Decays : The BHLS₂ Dipion Mass Spectra	13
9	Final State Interaction (FSI) in the η/η' Radiative Decays	14
10	Fits of the η/η' Radiative Decay Spectra within BHLS₂	19
	10.1 Available Dipion Spectra from the $\eta/\eta' \rightarrow \pi^+ \pi^- \gamma$ Decays	20
	10.2 η/η' Experimental Spectra : Fits in Isolation	21
	10.3 The η/η' Experimental Spectra : Analysis within the BHLS ₂ Context	22
	10.4 Final State Interaction: BHLS ₂ Fit Results versus Others	26
	10.5 The $T^{R2}(\eta/\eta')$ Terms in BHLS ₂ : The Role of ρ^\pm Exchanges	30
	10.6 Dealing with the Absolute Scale of the η/η' dipion spectra	32
11	η/η' Decays : The Muon Anomalous Magnetic Moment	33
	11.1 Accuracy of the FSI Parametrization	34
	11.2 The η/η' Spectra and HVP Estimates	38
	11.3 η/η' Based Evaluations of the HVP	38
12	Concluding Remarks	39
A	Brief Outline of the HLS/BHLS₂ Approach	40
	A.1 The Unbroken Non-Anomalous HLS Lagrangian	41
	A.2 Breaking the HLS Lagrangian I : The BKY Mechanism	42
	A.3 Breaking the HLS Lagrangian II : The Covariant Derivative (CD) Breaking	42
	A.4 Breaking the HLS Lagrangian III : Dynamical Vector Meson Mixing	43
	A.5 The Kinetic Breaking and the $[\pi^0, \eta, \eta']$ System	44
B	Erratum : The VPP/APP interaction pieces in BHLS₂	46

C	A_{\pm} Solutions : The <i>AAP</i> and <i>VVP</i> Lagrangians	46
C.1	The <i>AAP</i> Lagrangian	47
C.2	The <i>VVP</i> Lagrangian	48
C.2.1	The <i>VVπ</i> Lagrangians	48
C.2.2	The <i>VVη</i> Lagrangian	49
C.2.3	The <i>VVη'</i> Lagrangian	49
D	A_{\pm} Solutions : The <i>APPP</i> and <i>VPPP</i> Lagrangians	50
D.1	The <i>APPP</i> Lagrangian	50
D.2	The <i>VPPP</i> Lagrangian	51
E	Brief Analysis of the BHLS₂ Parameters Values	51

1 Preamble : Various Aspects of the Dispersive Approach to the Muon HVP

The hadronic vacuum polarization (HVP) $a_{\mu} \equiv (g_{\mu} - 2)/2$ plays a central role in precision physics, in particular, in the Standard Model prediction of the Muon Anomalous Magnetic Moment, but as importantly, for a precise calculation of the running electromagnetic fine structure constant $\alpha_{em}(s)$ and of the electroweak mixing parameter $\sin^2 \theta_W(s)$. Thereby, accurate predictions suffer from the non-perturbative contributions from the low-lying hadron physics uneasy to address precisely from first principles.

Recently [2], the Muon $g - 2$ FNAL experiment has re-estimated the previous average value of their run 1 data sample [2] and the latest BNL measurement [4] by also considering their run 2 and 3 data samples; this turns out to increase the statistics by a factor of $\simeq 4$. Moreover, the Muon $g - 2$ FNAL Collaboration achieved an improvement by about a factor of 2 of their systematics uncertainty. The derived updated average :

$$a_{\mu}^{exp.} = 116592059(22) \times 10^{-11}(0.19\text{ppm})$$

increases the deviation from the White Paper(WP) Standard Model consensus [3], from 4.2σ [1] to 5.0σ [2]. The difference $\delta_a = a_{\mu}^{exp.} - a_{\mu}^{th.}$ is now $\delta_a = 24.4 \pm 4.5$ in units of 10^{-10} , dominated by the uncertainty agreed upon by the WP theory consensus [3]. This departure from theoretical expectations deserves, of course, to be explored as, indeed, the overall pattern reflected by the various model/theoretical approaches is unclear, even contradictory.

The WP Standard Model consensus for $a_{\mu}^{th.}$ resorts to a data-driven dispersion relation (DR) approach, where the experimental low-energy hadron production cross-sections provide the non-perturbative input to calculate the HVP effects. Fortunately, the problem can be restricted to a precise knowledge of the process $e^+e^- \rightarrow \gamma^* \rightarrow$ hadrons, and for what concerns the muon $g - 2$, the $e^+e^- \rightarrow \pi^+\pi^-$ channel provides the dominant contribution to the model uncertainty.

Regarding its non-perturbative hadronic content, the standard DR based evaluation of the HVP consists in deriving the contribution of *each* $e^+e^- \rightarrow \gamma^* \rightarrow$ hadrons annihilation channel

by combining the different spectra collected by the different experiments in the hadronic channel considered by means of algorithms of different levels of sophistication. The full hadronic HVP value is then defined, for what concerns its non-perturbative content, by the sum of these different contributions. The WP Standard Model consensus [3] is based on a combination of two such evaluations [5, 6].

Although the main challenge is then, seemingly, the simple $\pi\pi$ -production process, the experimental challenge is highly complex depending on a precise understanding of the detectors and, on the theory side, on the radiative corrections required to disentangle hadronic effects from electromagnetic contamination. Unfortunately, the data samples provided by the different experiments do not exhibit a satisfactory consistency – and even some can be in strong contradiction [7] with the others. Using the $\tau \rightarrow \pi^- \pi^0 \nu_\tau$ decay information, first proposed by [8], has been considered to discriminate among the $\pi^+ \pi^-$ spectra, but did not lead to convincing enough conclusions.

It is widely considered that all low-energy hadronic processes derive from QCD even though, in the non-perturbative low-energy regime, tools to make valid predictions of real-time hadronic cross sections are missing. Nevertheless, as hadron physics is accepted to derive from QCD, it follows that *the various specific hadronic decay processes are highly correlated to each other*. It is thus motivated to address these correlations, especially in order to constrain the non-perturbative sector of the $e^+e^- \rightarrow \gamma^* \rightarrow$ hadrons annihilations.

Although we lack methods to predict a process like $e^+e^- \rightarrow \pi^+\pi^-$, we know that QCD implies well-defined symmetry patterns like approximate chiral symmetry, and gives rise to Chiral Perturbation Theory (ChPT), a systematic expansion about the chiral symmetry point. It allows one to work out reliable predictions from first principles for the low energy tail of the QCD hadron spectrum (up to about the η meson mass).

With this in mind, an attempt to consider the $e^+e^- \rightarrow \pi^+\pi^-$ annihilation not only in relation with the $\tau^\pm \rightarrow \pi^\pm \pi^0 \nu_\tau$ decay *but also with other related spectra* is important; it motivates a unified modeling¹ by a version of the Resonance Lagrangian approach (RLA) – we adopted the Hidden Local Symmetry (HLS) version [9, 10] – needed to extend Chiral perturbation theory towards higher energy to cover the ρ , ω and ϕ energy range². To practically succeed in such a program, the original HLS model – see for instance [13] for a review – has been supplied with appropriate symmetry breaking mechanisms with various levels of sophistication to derive the earlier versions of the BHLS model as [14, 15, 16], or the more refined BHLS₂ version [17], updated in [18].

One thus achieved a simultaneous consistent fit of the $e^+e^- \rightarrow \pi^+\pi^-$ data from CMD-2 [19], SND [19], KLOE [13,14,15], BaBar [16,17], BESIII [67,68] and CLEO-c [20] and the $\tau \rightarrow \pi^- \pi^0 \nu_\tau$ decay spectral functions collected by ALEPH [21], CLEO [22] and Belle [23] (see [14, 15, 17, 18]). This updated BHLS₂ fairly recovers the known properties of the $[\pi^0, \eta, \eta']$

¹Considering individual channels in isolation, as usually done, does not help much to uncover inconsistencies between different experimental data sets sometime involving different final states.

²A precise evaluation of the photon HVP implies a precise account of the energy range $\sqrt{s} \equiv [2m_\pi, 1.05 \text{ GeV}]$, the largest contribution of the non-perturbative region which extends up to $\simeq 2 \text{ GeV}$ as experimentally observed [11, 12].

system thanks to its kinetic breaking mechanism [18].

Beside keeping the neutral vector current conserved, this breaking mechanism also generates a violation of the charged vector current conservation and a departure of $F_\pi^T(s=0) = 1$ by a few per mil. Such an option finds a support in the own Belle fit results reported in Table VII of their [23]; additional τ spectra are needed to conclude – see the discussion in Section 3 of [18] – as such a breaking mechanism might affect τ based predictions for the muon HVP.

Beside the $\pi^+\pi^-$ annihilation channel and the $\tau \rightarrow \pi^-\pi^0\nu_\tau$ decay spectra, BHLS₂ [17, 18], also addressed successfully the $\pi^+\pi^-\pi^0$, $(\pi^0/\eta)\gamma$ and $K\bar{K}$ final states in the fully correlated way represented by a single Lagrangian. A few additional radiative partial width decays are also considered, noticeably those for $\pi^0/\eta/\eta' \rightarrow \gamma\gamma$, and some more $VP\gamma$ radiative decays.

In view of the significant inconsistencies of the data samples collected by some experiments, the global fit approach has two advantages: first, more data are expected to reduce the uncertainties of the HVP evaluations and, second, provides consistency checks of each $e^+e^- \rightarrow \gamma^* \rightarrow$ hadrons data set versus the other samples collected in the same annihilation channel *or in another one*.

In the present work, we go a step further by also involving the $\eta/\eta' \rightarrow \pi^+\pi^-\gamma$ decay modes in order to obtain additional $\pi\pi$ dipion spectra from experiments with systematics quite different from those encountered in e^+e^- annihilations. As will be seen below, these decays allow for a new test of the self-consistency of the DR based estimates of a_μ : Indeed, the η/η' decay spectra can provide a DR evaluation for $a_\mu(\pi^+\pi^-, \sqrt{s} < 1 \text{ GeV})$ which can be fruitfully compared with those directly derived from directly integrating the $e^+e^- \rightarrow \pi^+\pi^-$ annihilation data. One may expect that the η/η' dipion spectra benefit from systematics largely independent of those in the e^+e^- annihilation.

Beside the DR approach which gave rise to several evaluations of the muon HVP a_μ listed in the White Paper [3], the challenging Lattice QCD (LQCD) approach has been used by several groups and produced results with relatively poor precision at the time of the White Paper. They were not used to define the so-called WP Standard Model consensus reported in [3] which, based on some DR estimates, provided the leading order (HVP-LO) consensus $a_\mu^{\text{LO}}[\text{th.}] = 693.1(4.0) \times 10^{-10}$. Using the LQCD approach, the BMW Collaboration which first got [24, 3] $a_\mu^{\text{LO}} = (711.1 \pm 7.5 \pm 17.4) \times 10^{-10}$ later on improved their calculation and got $a_\mu^{\text{LO}} = (707.5 \pm 5.5) \times 10^{-10}$ [25] at clear variance with the WP consensus just reminded. This evaluation finds support from the new evaluations by other LQCD groups: $a_\mu^{\text{LO}} = (720.0 \pm 12.4_{\text{stat}} \pm 9.9_{\text{syst}}) \times 10^{-10}$ (Mainz/CLS 19) and $a_\mu^{\text{LO}} = (715.4 \pm 16.3_{\text{stat}} \pm 9.2_{\text{syst}}) \times 10^{-10}$ (RBC/UKQCD18) [26] [78].

The lattice calculation of a_μ^{LO} thus brings the SM prediction of a_μ into an acceptable agreement with the experiment but generates a significant disagreement between the LQCD results and the different data-driven dispersive results; this looks now well established. It moves the former puzzle from data versus predictions to a puzzle between Lattice QCD and the DR approaches which deserves clarification.

2 Introduction

In this article, we focus on the traditional way to estimate the contribution of the non-perturbative energy region to the photon HVP which relies on dispersive methods using as basic ingredients the e^+e^- annihilation cross sections to all the possible exclusive hadronic final states collected up to $\sqrt{s} \simeq 2$ GeV.

The different successive broken variants of the HLS model, especially BHLS₂ [17, 18], provides a well adapted framework to address the most relevant e^+e^- annihilations to hadronic channels in the crucial part of the low energy region ($\sqrt{s} \leq 1.05$ GeV), namely the e^+e^- annihilations to the $\pi^+\pi^-$, $K\bar{K}/\pi^+\pi^-\pi^0/\pi^0\gamma/\eta\gamma$ final states; these already provide more than 80% of the muon HVP, when integrated up to the ϕ meson mass.

A BHLS₂ based computer code was used for this analysis which considered the large number of available data samples (several dozens), more than 1400 data points and thus, practically, the whole set of the available data samples has been exhausted. They have been listed, analyzed and discussed in full details previously, especially in the recent articles [17, 18], where a large number of previous references can be found³. This computer code takes faithfully into account the whole uncertainty information provided together with these data samples and, therefore, yielding satisfactory global fit probabilities turns out to have simultaneously a satisfactory model, a satisfactory handling data of the samples collected in several physics channels and, also, a satisfactory dealing with their reported uncertainty information.

In this perspective, given data samples exhibiting contradictory aspects compared to most of the others may lead to either discard them or, when meaningful, motivate several solutions which avoids to mix up contradictory spectra; this has led us in our previous studies [17, 18] to provide different HVP evaluations based on some of the reported dipion KLOE samples, – namely [27, 28, 29] – on the one hand and separately on their Babar analog [30, 31] on the other hand.

Regarding the various dipion spectra, the studies finding strong contradictions between the so-called KLOE8 data sample [32], or the recently published SND spectrum [33], and the bulk of the other considered data samples, have been discarded.

Comparing our own evaluations with those based on Dispersion Relations collected in [3], one does not observe any loss in precision with any of the various reported values of the muon $g - 2$; however, differences between central values can be observed, clearly related with the contradictory properties of some data samples, especially KLOE [27, 28] versus Babar [30, 31] reported since a long time [15, 16, 34].

As noted above, the contribution of the listed HLS channels to the HVP is large; however, it is also worth mentioning that their contribution to the HVP uncertainty is almost negligible compared to those of the rest of the non-perturbative region. Moreover, as the HLS approach

³ The CMD-3 Collaboration has recently published a high statistics measurement of the $e^+e^- \rightarrow \pi^+\pi^-$ cross section [7] which deserves a specific analysis beyond the scope of the present work which is focused on a quite different topic; nevertheless, the information provided by the CMD-3 Collaboration in their article regarding the consistency of their spectrum with the previously collected data samples may indicate that, as it is, their measurement is not consistent with any subset of the relevant existing data samples and thus it should hardly accommodate a global framework like HLS; so, it should not impact the conclusions of the present work.

implies tight connexions between the various annihilation channels, it allows performing stringent consistency checks on the different data samples involving the same physics channels or, also, the other channels addressed by the HLS Lagrangian. It is worthwhile pointing out this important property, specific to global models like BHLS₂ and also stressing that, by far, most of the available data samples fulfill this drastic constraint.

On the other hand, as indicated in the previous Section, the updated variant BHLS₂ variant [18] of the broken HLS model [17] allows to fairly address the physics of the [π^0 , η , η'] system within the HLS corpus. Indeed, beside the $e^+e^- \rightarrow (\pi^0/\eta)\gamma$ annihilations, the PS decays to $\gamma\gamma$ and the $VP\gamma$ couplings, the pseudoscalar meson (PS) mixing properties in the octet-singlet [35, 36, 37] and quark flavor [38, 39, 40] basis parametrizations have been analyzed, leading to a satisfactory comparison with expectations.

Among the other processes involving the properties of the [π^0 , η , η'] system, the $\eta' \rightarrow \pi^+\pi^-\gamma$ decay spectrum deserves a special attention. The measurements of this decay process started long ago – as early as 1975 [41] – and several experiments have collected samples of limited statistics [42, 43, 44, 45, 46, 47, 48, 49] motivated by a reported 20 MeV mass shift of the ρ peak compared to its observed value in the $e^+e^- \rightarrow \pi^+\pi^-$ annihilation.

This effect was soon attributed to an interference between the $\eta' \rightarrow \rho\gamma$ ($\rho \rightarrow \pi^+\pi^-$) resonant amplitude and the Wess-Zumino-Witten (WZW) anomalous $\eta'\pi^+\pi^-\gamma$ contact term [50, 51]; this so-called box anomaly was expected to occur alongside the triangle anomaly responsible of the two-photon decays of the π^0 , η and η' mesons. A basic HLS approach including this anomalous interaction term beside the dominant $\eta'\rho^0\gamma$ coupling [52] confirmed this guess.

However, the dipion η' spectrum from BESIII Collaboration [53] published much later, thanks to its large statistics (970,000 events), modified the picture : It led to conclude that supplementing the (ρ^0 , ω) resonance contributions by only a contact term is insufficient to reach a satisfactory description of the dipion spectrum.

On the other hand, the reported dipion spectrum observed in the parent $\eta \rightarrow \pi^+\pi^-\gamma$ decay has undergone much less measurements. Beside former spectra⁴ from Layter *et al.* [54] and Gormley *et al.* [55], WASA-at-COSY reported for a 14,000 event spectrum [56] whereas the KLOE/KLOE2 Collaboration collected a 205,000 event spectrum [57].

As the dipion spectra reported from the recent measurements of the $\eta/\eta' \rightarrow \pi^+\pi^-\gamma$ decays carry high statistics, it thus becomes relevant to re-examine if (and how) they fit within the recently defined BHLS₂ framework of the HLS model, especially thanks to its kinetic breaking (See Appendix A.5) which has already allowed for a satisfactory description of the [π^0 , η , η'] system properties [18]. Moreover, even if the physics of the η/η' mesons is interesting *per se*, a better understanding of their properties is important, given their important role in the Light-by-Light (LbL) contribution to the muon anomalous magnetic moment.

The layout of the paper is as follows. Section 3 aims at reminding the Kroll conditions [58] which reduce the number of free parameters of the kinetic breaking mechanism from 3 to 1; it

⁴The numerical content of these spectra can only be derived from the paper figures.

also reminds and corrects Lagrangian pieces relevant for the present study. Section 4 is intended to identify the Lagrangian pieces contributing to the considered η and η' radiative decays and displays the involved diagrams; the BHLS₂ amplitudes for these are constructed in Section 5 for the $\eta \rightarrow \pi^+\pi^-\gamma$ decay and in Section 6 for the $\eta' \rightarrow \pi^+\pi^-\gamma$ one. The relation between the anomalous HLS amplitudes and their Wess–Zumino–Witten (WZW) [50, 51] analogs is given in Section 7. The derivation of the dipion mass spectrum in the η/η' radiative decays is done in Section 8 and the role of the final state interaction mechanism (FSI) in the η/η' radiative decays is thoroughly examined in Section 9.

Section 10 is the central part of the present study; Subsection 10.1 presents exhaustively the available $\eta/\eta' \rightarrow \pi^+\pi^-\gamma$ data samples; for this purpose it is important to note that all the available spectra carry an arbitrary absolute normalization and that, accounting for the $\eta/\eta' \rightarrow \pi^+\pi^-\gamma$ partial widths implies using also an external piece of (PDG [59]) information. A detailed study of the FSI polynomial degrees is the subject of Subsection 10.2 which reports on the fits performed separately with the η and η' spectra to find the appropriate degrees of the requested FSI polynomials. This permits to perform the fits of the dipion spectra reported in Subsection 10.3 where it is proved that a unique FSI polynomial can satisfactorily account for both the η and η' dipion spectra simultaneously.

Subsection 10.4 is devoted to comparing our FSI polynomial results to those reported in the literature. The role of intermediate ρ^\pm exchanges is emphasized in Subsection 10.5. The global BHLS₂ fits performed to simultaneously describe the dipion spectrum lineshapes examined in the previous Subsections and the PDG information for the partial widths $\Gamma(\eta/\eta' \rightarrow \pi^+\pi^-\gamma)$ is worked out in Subsection 10.6. Finally in Section 11 one examines the issues relative to the connection between the $\eta/\eta' \rightarrow \pi^+\pi^-\gamma$ decays and the hadronic contribution to the muon anomalous magnetic moment a_μ . Section 12 summarizes the conclusions reached by the present study.

In order to ease the paper reading, the main pieces of information regarding the HLS model are briefly reminded in Appendix A.1, whereas its symmetry breaking mechanisms are briefly summarized in Appendices A.2 to A.5. An Erratum to the previous broken version of the BHLS₂ version is the subject of Appendix B. To ease the reading of the present work, one has also found appropriate to give the most relevant parts of the non–anomalous and anomalous BHLS₂ pieces under the Kroll Conditions – reminded just below – in Appendices C and D. A brief numerical analysis of some parameter values returned by the fits of the η/η' dipion spectra is the subject of Appendix E.

3 The Kroll Conditions and VPP Lagrangian Pieces

In the FKS approach [38, 39, 40] to the $[\pi^0, \eta, \eta']$ system, it has been found appropriate to impose the Kroll conditions [58] to axial current matrix elements. Applied to the BHLS₂ axial currents, these conditions :

$$\langle 0 | J_\mu^a | \eta_b(p) \rangle = i p_\mu f_a \delta_{ab} \quad , \quad | \eta_b(p) \rangle = | b\bar{b}(p) \rangle \quad , \quad J_\mu^a = \bar{a} \gamma_\mu \gamma_5 a \quad , \quad \{a, b = u, d, s\} \quad . \quad (1)$$

lead to two non-trivial relations [18] – referred to below as A_{\pm} solutions – among the λ_i parameters of the generalized 't Hooft term [60, 37] (see Appendix B); one gets :

$$\left\{ \text{Solutions } A_{\pm} \iff \lambda_0 = \sqrt{2}\lambda_8 = \pm\sqrt{\frac{3}{2}}\lambda_3 \right\}. \quad (2)$$

which reduces the actual parameter freedom of the kinetic breaking from three to only one.

One thus should note that the Kroll Conditions tightly couple the breaking in the BHLS₂ Lagrangian of the original U(3) symmetry to SU(3)×U(1) and a particular Isospin breaking piece (via $\lambda_3 \neq 0$); it also lead to $F_{\pi}^{\tau}(s=0) = 1 - \lambda_3^2/2$.

The ± 1 factor in Equations (2) is propagated below as d_{\pm} ; so, A_+ corresponds to d_+ and A_- to d_- . The non-anomalous pieces $\mathcal{L}_{\eta'\pi^{\pm}}$ and $\mathcal{L}_{\eta\pi^{\pm}}$ of the BHLS₂ Lagrangian acquire simplified expressions compared to [18] :

$$\left\{ \begin{array}{l} \mathcal{L}_{\pi^0\pi^{\pm}} = \frac{ia g}{2}(1 + \Sigma_V)\left(1 - \frac{\lambda_0^2}{3}\right) \left[\rho^- \cdot \pi^+ \overset{\leftrightarrow}{\partial} \pi^0 - \rho^+ \cdot \pi^- \overset{\leftrightarrow}{\partial} \pi^0 \right] \\ \mathcal{L}_{\eta\pi^{\pm}} = -\frac{ia g}{2} [1 + \Sigma_V] \left[\epsilon - \frac{A_{\pm}}{2} \sin \delta_P \right] \left[\rho^- \cdot \pi^+ \overset{\leftrightarrow}{\partial} \eta - \rho^+ \cdot \pi^- \overset{\leftrightarrow}{\partial} \eta \right] \\ \mathcal{L}_{\eta'\pi^{\pm}} = -\frac{ia g}{2} [1 + \Sigma_V] \left[\epsilon' + \frac{A_{\pm}}{2} \cos \delta_P \right] \left[\rho^- \cdot \pi^+ \overset{\leftrightarrow}{\partial} \eta' - \rho^+ \cdot \pi^- \overset{\leftrightarrow}{\partial} \eta' \right] \end{array} \right. \quad (3)$$

where :

$$A_{\pm} = \Delta_A + d_{\pm}\lambda_0^2, \quad (4)$$

exhibiting the BKY Δ_A and δ_P is defined by :

$$\cos \delta_P = \frac{1}{\sqrt{3}} \left[\sin \theta_P + \sqrt{2} \cos \theta_P \right], \quad \sin \delta_P = -\frac{1}{\sqrt{3}} \left[\cos \theta_P - \sqrt{2} \sin \theta_P \right] \quad (5)$$

in terms of θ_P , the third mixing angle [61] which is one among the BHLS₂ fit parameters. It has been shown in [18] that the BKY parameter Σ_V can be dropped out without any loss in generality.

One should note that, if $\mathcal{L}_{\pi^0\pi^{\pm}}$ is leading order, both $\mathcal{L}_{\eta\pi^{\pm}}$ and $\mathcal{L}_{\eta'\pi^{\pm}}$ are manifestly $\mathcal{O}(\delta)$, *i.e.* first order in breakings. Finally, it is worthwhile to remind that terms of order $\mathcal{O}(\delta^2)$ or higher in amplitudes are discarded.

4 The $\eta/\eta' \rightarrow \pi^- \pi^+ \gamma$ Decays in the BHLS₂ Framework

The amplitudes for the $\eta/\eta' \rightarrow \pi^- \pi^+ \gamma$ decays *a priori* involve the *APPP*, *VPPP* and *AVP* sectors of the full BHLS₂ Lagrangian [17, 18]. The interaction terms involved are displayed in Appendices C and D in terms of the *physical* pseudoscalar fields and *ideal* vector fields which should be replaced by their physical partners following the method developed in [17]. The $V - \gamma$ transition couplings can be found in [17], Appendix A and the relevant

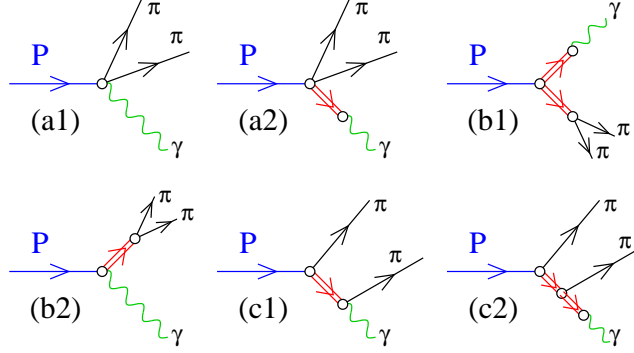


Figure 1: The classes of tree diagrams. P stands for either of η and η' ; in diagrams a and b , the double lines stand for the neutral vector mesons (subject to mixing), in diagrams c , the intermediate vector meson is ρ^\pm whereas the external one is neutral. The pions are charged. The vanishing of the AVP couplings (see text) implies that diagrams (b2) and (c1) do not contribute to the decay amplitudes.

non-anomalous VPP couplings have been displayed, for convenience, in Section 3 just above. The classes of diagrams *a priori* involved in the η/η' decays to $\pi^-\pi^+\gamma$ are displayed in Figure 1. Namely, diagram (a1) illustrates the $AVPP$ interaction, whereas diagram (a2) sketches the $VPPP$ contributions with $V-\gamma$ transitions ($V = \rho^0, \omega, \phi$) provided by the non-anomalous $BHLS_2$ Lagrangian ([17], Appendix A). These two kinds of diagrams are generally named box anomaly terms.

Diagram (b1) sketches the diagram class involving VVP couplings; these diagrams provide the major contribution to the η/η' dipion spectra. As one assumes $c_3 = c_4$ thanks to former works [15], all contributions involving AVP couplings, as those depicted in Figures (b2) and (c1), identically vanish. Finally, the (c2) diagram class illustrates the diagrams reflecting the 2 possible choices for the $\pi^\pm\pi^\mp$ pair, each involving an intermediate ρ^\pm exchange.

In the following, for the η and η' decays, the non-resonant (a1) and (a2) contributions are gathered into the T^{NR} partial amplitude, whereas the (b1) and (c2) resonant contributions are given by resp. the T^{R1} and T^{R2} terms.

5 The $\eta \rightarrow \pi^+\pi^-\gamma$ Amplitude within $BHLS_2$

As three kinds of diagrams contribute, the full $T(\eta)$, amplitude for the $\eta \rightarrow \pi^+\pi^-\gamma$ decay is written :

$$T(\eta) = T^{NR}(\eta) + T^{R1}(\eta) + T^{R2}(\eta) \quad (6)$$

and they include the common tensor object :

$$F = \epsilon^{\mu\nu\alpha\beta} \epsilon_\mu(\gamma, q) q_\nu p_\alpha^- p_\beta^+ \quad (7)$$

typical of the anomalous Lagrangian piece expressions; F exhibits the obvious momentum notations. This factor is understood in the $T(\eta/\eta')$ amplitude expressions here and below to lighten writing; it is restored in the final expressions involving the differential decay widths.

As already stated, the first term in the expansion (6) gathers the non-resonant ($APPP/VPPP$) contributions whereas the second and third terms collect the resonant contributions of different structure generated via the VVP Lagrangian and commented in the Section just above.

The T_{NR}^η term can be written ($A_\pm = \Delta_A + d_\pm \lambda_0^2$) :

$$T^{NR}(\eta) = -\frac{ie}{4\pi^2 f_\pi^3} \left[1 - \frac{3c_3}{2} \right] g_{\eta\pi^+\pi^-\gamma} \quad \text{with} \quad g_{\eta\pi^+\pi^-\gamma} = \epsilon + \left\{ 1 - \frac{A_\pm}{2} - \frac{3\lambda_0^2}{4} \right\} \sin \delta_P . \quad (8)$$

It is worthwhile noting that i/ The dependency upon $c_1 - c_2$ drops out when summing up the $APPP$ and $VPPP$ contributions, ii/ If one cancels out the symmetry breaking contributions, $T^{NR}(\eta)$ remains non-zero and corresponds to the Wess-Zumino-Witten (WZW) term [50, 51].

On the other hand, the $T^{R1}(\eta)$ contributions to the $T(\eta)$ amplitude can be written ($m^2 = ag^2 f_\pi^2$) :

$$\left\{ \begin{array}{l} T^{R1}(\eta) = c_3 \frac{iem^2}{8\pi^2 f_\pi^3} \left[\frac{T_\rho^0(\eta)}{D_\rho(s)} + \frac{T_\omega^0(\eta)}{D_\omega(s)} + \frac{T_\phi^0(\eta)}{D_\phi(s)} \right] \\ T_\rho^0(\eta) = \epsilon + \frac{2\beta(s)}{z_A} \cos \delta_P + 3 \left[1 - \frac{3\lambda_0^2}{4} - \frac{A_\pm}{6} + \frac{\alpha(s)}{3} + 2\xi_3 \right] \sin \delta_P \\ T_\phi^0(\eta) = - \left[\frac{2\beta(s)}{z_A} \right] \cos \delta_P \\ T_\omega^0(\eta) = - \alpha(s) \sin \delta_P \end{array} \right. \quad (9)$$

where $D_\rho(s)$, $D_\omega(s)$ and $D_\phi(s)$ are the indicated inverse vector meson propagators; they are parametrized as defined in Section 9 of [17]. Equations (9) displays the dependency upon the angles $\alpha(s)$ and $\beta(s)$ defining the dynamical vector meson mixing (see Appendix A.4) and upon the parameter defined by the kinetic breaking mechanism (see Appendix A.5), once the Kroll conditions [58] are applied. It is worth remarking that ρ^0 is the only resonant contribution which survives when symmetry breaking terms are turned off. Moreover, the ω and ϕ contributions are outside the phase space actually available in the η decay.

$T^{R2}(\eta)$, the second resonant contribution, is produced by the *non-anomalous* $\rho^\pm \eta \pi^\mp$ coupling purely generated by our breaking procedures (see Equations (3)) and by the $\omega \rho^\pm \pi^\mp$ term of the $VV\eta$ Lagrangian piece (see Appendix C.2.2). Setting :

$$s_{\pm 0} = (p_\pm + q)^2 \quad , \quad q = \text{photon momentum} \quad ,$$

it writes:

$$\begin{cases} T^{R2}(\eta) = c_3 \frac{iem^2}{8\pi^2 f_\pi^3} T_\rho^\pm(\eta) \left[\frac{1}{D_\pm(s_{+0})} + \frac{1}{D_\pm(s_{-0})} \right] \\ T_\rho^\pm(\eta) = \epsilon - \frac{A_\pm}{2} \sin \delta_P. \end{cases} \quad (10)$$

The $D_\pm(s_{\pm 0})$'s denoting the inverse ρ^\pm propagators; the T^{R2} contribution, a pure product of symmetry breakings, cancels out when all symmetries are restored. Finally, the 3 amplitudes pieces just defined depend on the HLS parameter c_3 .

At the chiral point

$$s = s_{+0} = s_{-0} = 0 ,$$

the vector meson inverse propagators fulfill [17] $D_V(0) = -m_V^2$ with :

$$m_{\rho_\pm}^2 = m^2 , \quad m_{\rho_0}^2 = m^2(1 + \xi_3)^2 , \quad m_\omega^2 = m^2(1 + \xi_0)^2 , \quad m_\phi^2 = m^2 z_V(1 + \xi_0)^2 . \quad (11)$$

where $m^2 = ag^2 f_\pi^2$, the conditions $\alpha(0) = \beta(0) = 0$ being exactly fulfilled.

6 The $\eta' \rightarrow \pi^+ \pi^- \gamma$ Amplitude within BHLS₂

The decay process $\eta' \rightarrow \pi^+ \pi^- \gamma$ undergoes a quite similar treatment to those performed for the $\eta \rightarrow \pi^+ \pi^- \gamma$ decay in the preceding Section and, so, one will avoid duplicating on the η' amplitude the comments already stated on the η amplitude. The three different kinds of contributions to the η' decay amplitude are :

$$T(\eta') = T^{NR}(\eta') + T^{R1}(\eta') + T^{R2}(\eta') . \quad (12)$$

The first term, which gathers the *APPP* and *VPPP* contributions to the full amplitude $T^{\eta'}$, is given by :

$$T^{NR}(\eta') = -\frac{ie}{4\pi^2 f_\pi^3} \left[1 - \frac{3c_3}{2} \right] g_{\eta' \pi^+ \pi^- \gamma} \quad \text{with} \quad g_{\eta' \pi^+ \pi^- \gamma} = \epsilon' - \left\{ 1 - \frac{A_\pm}{2} - \frac{3\lambda_0^2}{4} \right\} \cos \delta_P \quad (13)$$

and does not depend on $c_1 - c_2$. On the other hand, the contributions gathered in $T^{R1}(\eta')$ are given by :

$$\begin{cases} T^{R1}(\eta') = c_3 \frac{iem^2}{8\pi^2 f_\pi^3} \left[\frac{T_\rho^0(\eta')}{D_\rho(s)} + \frac{T_\omega^0(\eta')}{D_\omega(s)} + \frac{T_\phi^0(\eta')}{D_\phi(s)} \right] \\ T_\rho^0(\eta') = \epsilon' + \frac{2\beta(s)}{z_A} \sin \delta_P - 3 \left[1 - \frac{3\lambda_0^2}{4} - \frac{A_\pm}{6} + \frac{\alpha(s)}{3} + 2\xi_3 \right] \cos \delta_P \\ T_\phi^0(\eta') = - \left[\frac{2\beta(s)}{z_A} \right] \sin \delta_P \\ T_\omega^0(\eta') = + \alpha(s) \cos \delta_P \end{cases} \quad (14)$$

where, as for the η decay, only the ρ^0 term is $\mathcal{O}(\delta^0 = 1)$ in breakings. Finally :

$$\begin{cases} T^{R2}(\eta') = c_3 \frac{iem^2}{8\pi^2 f_\pi^3} T_\rho^\pm(\eta') \left[\frac{1}{D_\pm(s_{+0})} + \frac{1}{D_\pm(s_{-0})} \right] \\ T_\rho^\pm(\eta') = \epsilon' + \frac{A_\pm}{2} \cos \delta_P. \end{cases} \quad (15)$$

which is purely $\mathcal{O}(\delta)$.

The ω contribution in the η' decay must be visible in high statistics data samples (like [53]) and worth to compare with its lineshape in the $e^+e^- \rightarrow \pi^+\pi^-$ annihilation. Regarding the ϕ contribution, it is somewhat outside of the allowed phase space – by $\simeq 60$ MeV. Finally, the influence of higher vector mesons, especially the first radial excitation ρ' , are outside the HLS scope; global fit properties may reveal their actual influence, w.r.t. the broken HLS context.

7 BHLS₂ and the WZW Box Anomalies

Traditionally, the amplitudes associated with the box anomalies are derived from the Wess-Zumino-Witten (WZW) Lagrangian [50, 51] :

$$\mathcal{L}_{WZW} = -i \frac{N_c e}{3\pi^2 f_\pi^3} \epsilon^{\mu\nu\alpha\beta} A_\mu \text{Tr} [Q \partial_\nu P \partial_\alpha P \partial_\beta P] . \quad (16)$$

where P is the bare pseudoscalar meson $U(3)$ matrix. This Lagrangian differs from the anomalous $APPP$ Lagrangian piece of the HLS model (see Equation (86)) by the factor

$$\left[1 - \frac{3}{4}(c_1 - c_2 + c_4) \right]$$

The BHLS₂ η/η' decay amplitudes just defined are expected to coincide with their WZW analogs at the chiral point, where the HLS c_i 's dependencies of the decay amplitudes should cancel out. Their expressions at the chiral point ($s = s_{+0} = s_{-0} = 0$) are given by⁵ :

$$\begin{cases} T(\eta) = -\frac{ie}{4\pi^2 f_\pi^3} \left[\epsilon + \left\{ 1 - \frac{A_\pm}{2} - \frac{3\lambda_0^2}{4} \right\} \sin \delta_P \right] , \\ T(\eta') = -\frac{ie}{4\pi^2 f_\pi^3} \left[\epsilon' - \left\{ 1 - \frac{A_\pm}{2} - \frac{3\lambda_0^2}{4} \right\} \cos \delta_P \right] , \\ T(\pi^0) = +\frac{ie}{4\pi^2 f_\pi^3} \left[\left\{ 1 - \frac{A_\pm}{2} - \frac{\lambda_0^2}{3} \right\} - \epsilon \sin \delta_P + \epsilon' \cos \delta_P \right] . \end{cases} \quad (17)$$

and coincide with those which can be directly derived from the WZW Lagrangian Equation (16) after applying the breaking procedures reminded in the Appendices.

⁵The coupling $\pi^0\pi^+\pi^-\gamma$ is involved in the $e^+e^- \rightarrow \pi^0\pi^+\pi^-$ annihilation [17, 18].

8 η/η' Radiative Decays : The BHLS₂ Dipion Mass Spectra

The amplitudes $T(\eta)$ and $T(\eta')$ allowing to describe – within the full EBHLS₂ framework [17, 18] – the dipion mass spectra observed in the η/η' radiative decays have been derived in resp. Sections 5 and 6; both should be multiplied by the function⁶ $F(s, s_{0+})$ (see Equation (7)). The differential decay widths can be written :

$$\frac{d^2\Gamma_X}{ds ds_{0+}} = \frac{1}{(2\pi)^3} \frac{1}{32M_X^3} |T_X F(s, s_{0+})|^2, \quad X = \eta, \eta' \quad (18)$$

in terms of resp. s , the $(\pi^+\pi^-)$ and s_{0+} , the $(\pi^+\gamma)$ pair invariant masses squared of the η/η' decay products. The accessible invariant mass spectra being functions of only s , this expression should be integrated over s_{0+} :

$$\frac{d\Gamma_X}{ds} = \frac{1}{(2\pi)^3} \frac{1}{32M_X^3} \int_{s_{min}}^{s_{max}} |T_X F(s, s_{0+})|^2 ds_{0+}, \quad X = \eta, \eta' \quad (19)$$

where :

$$s_{min/max} = \frac{M_X^2 + 2m_\pi^2 - s}{2} \mp p_\pi \frac{M_X^2 - s}{\sqrt{s}} \quad \text{and} \quad p_\pi = \frac{\sqrt{s - 4m_\pi^2}}{2}. \quad (20)$$

Both amplitudes $T(\eta)$ and $T(\eta')$, generically referred to as T_X , can be written :

$$T_X(s, s_{0+}) = R_X(s) + C_X G(s, s_{0+}) \quad \text{with} \quad G(s, s_{0+}) = \frac{1}{D_\rho(s_{0-})} + \frac{1}{D_\rho(s_{0+})}, \quad (21)$$

having defined $s_{0\pm} = (q + p^\pm)^2$ related by :

$$s_{0-} - m_\pi^2 = (M_X^2 - s) - (s_{0+} - m_\pi^2).$$

$R_X(s)$ collects the contributions previously named $T^{NR}(X)$ and $T^{R1}(X)$ and is (by far) the dominant term, whereas⁷ $T^{R2}(X) = C_X G(s, s_{0+})$ is only $\mathcal{O}(\delta)$ in breakings.

On the other hand, the $[F(s, s_{0+})]^2$ factor in Equation (19) is :

$$[F(s, s_{0+})]^2 = \frac{s}{4} (s_{0+} - m_\pi^2)(s_{0-} - m_\pi^2) - \frac{m_\pi^2}{4} (M_X^2 - s)^2 \quad (22)$$

and can be solely expressed in terms of s and s_{0+} to perform the integration shown in Equation (19). This leads to *predefine* within the fitting code the following integrals :

$$\begin{aligned} I_1(s) &= \int_{s_{min}}^{s_{max}} |F(s, s_{0+})|^2 ds_{0+}, & I_2(s) &= \int_{s_{min}}^{s_{max}} |F(s, s_{0+})|^2 |G(s, s_{0+})|^2 ds_{0+} \\ I_3(s) &= \int_{s_{min}}^{s_{max}} |F(s, s_{0+})|^2 \mathbf{Re}[G(s, s_{0+})] ds_{0+}, & I_4(s) &= \int_{s_{min}}^{s_{max}} |F(s, s_{0+})|^2 \mathbf{Im}[G(s, s_{0+})] ds_{0+} \end{aligned} \quad (23)$$

⁶The notations $\epsilon(\gamma, q)$ for the photon polarization vector, p^\pm and q for the pion and photon momenta are generally understood.

⁷ C_X can be read off the relevant expressions for $T^{R2}(X)$ given in Sections 5 and 6.

Actually, $I_1(s)$ can be integrated in closed form :

$$I_1(s) = \frac{(M_X^2 - s)^3 p_\pi^3}{3 \sqrt{s}} \quad (24)$$

with p_π given in Equations (20). The 3 other functions should be integrated numerically within the iterative procedure context already running to address the $e^+e^- \rightarrow \pi^+\pi^-\pi^0$ annihilation data within the BHLS [15] or BHLS₂ [17, 18] frameworks. One then gets :

$$\frac{d\Gamma_X}{ds} = \frac{1}{(2\pi)^3} \frac{1}{32M_X^3} \left[|R_X(s)|^2 I_1(s) + C_X^2 I_2(s) + 2C_X (\mathbf{Re} [R_X(s)] I_3(s) + \mathbf{Im} [R_X(s)] I_4(s)) \right] \quad (25)$$

In the BHLS₂ approach, only leading order terms in the breaking parameters $\mathcal{O}(\delta)$ (as the C_X term) are addressed and then terms of order $\mathcal{O}(\delta^2)$ – like the C_X^2 contribution – can be neglected.

The $I_1(s)$ term in Equation (25) can be rewritten, for subsequent use in the text :

$$\frac{d\tilde{\Gamma}_X}{ds} = \Gamma_0(s) |R_X(s)|^2, \quad \text{with } \Gamma_0(s) = \frac{s(M_X^2 - s)^3 [\sigma_\pi(s)]^3}{3 \cdot 2^{11} \pi^3 M_X^3} \quad \text{and } \sigma_\pi(s) = \sqrt{1 - \frac{4m_\pi^2}{s}}. \quad (26)$$

9 Final State Interaction (FSI) in the η/η' Radiative Decays

The study in [62], also referred to hereafter as SHKMW, has placed a valuable emphasis on the connection between the pion vector form factor $F_\pi(s)$ – as it comes out of the $e^+e^- \rightarrow \pi^+\pi^-$ annihilation process – and the dipion spectra from the $\eta/\eta' \rightarrow \pi^+\pi^-\gamma$ radiative decays. Further works have followed – see, for instance, [63, 64, 65, 66] for further references – generally motivated by a better understanding of the η and η' meson properties regarding their contributions to the light-by-light (LbL) fraction of the muon anomalous magnetic moment a_μ .

i) It is worthwhile to briefly outline how this connection is established [62]. The pion vector form factor $F_\pi(s)$ and the P -wave $\pi^+\pi^-$ scattering amplitude $T_{\pi\pi}(s)$ are related by :

$$\mathbf{Im} [F_\pi(s)] = \sigma_\pi(s) [T_{\pi\pi}(s)]^* F_\pi(s) \Theta(s - 4m_\pi^2), \quad (27)$$

valid along the energy region where the $\pi^+\pi^-$ scattering is *elastic*; $\sigma_\pi(s)$ has been defined just above. Therefore, in this energy region, the pion vector form factor $F_\pi(s)$ and the elastic scattering amplitude $T_{\pi\pi}(s)$ should carry equal phases. The Heaviside function indicates that $F_\pi(s)$ is real below the 2π threshold; the first *significant* inelastic channel being $\omega\pi$, the validity range of Equation (27) practically extends up to $\simeq 922$ MeV, much above the η mass and slightly below the η' mass (by only 36 MeV). Stated otherwise, the phase equality property holds over almost the whole HLS energy range of validity ($\sqrt{s} \leq 1.05$ GeV).

On the other hand, assuming the $\pi^+\pi^-$ scattering is elastic for all $s \geq 4m_\pi^2$, the P -wave amplitude $T_{\pi\pi}(s)$ writes :

$$T_{\pi\pi}(s) = \frac{\sin \delta_{11}(s)e^{i\delta_{11}(s)}}{\sigma_\pi(s)} \quad (28)$$

in terms of the P -wave phase shift $\delta_{11}(s)$ and the solution to Equation (27) can be expressed in terms of the Omnès function $\Omega(s)$ by :

$$F_\pi(s) = K(s)\Omega(s) \text{ , where } \Omega(s) = \exp \left(\frac{s}{\pi} \int_{4m_\pi^2}^{\infty} \frac{dz}{z} \frac{\delta_{11}(z)}{z-s-i\epsilon} \right) \text{ ,} \quad (29)$$

$K(s)$ being some appropriate real-analytic function, required to be free of singularities over the physical region $s \geq 4m_\pi^2$. This expression intends to factor out the non-perturbative contribution to $F_\pi(s)$ which is also contained in the $\Omega(s)$ function, and so the remaining part $K(s)$ is expected to behave smoothly and be well approximable by a polynomial [62] along our region of interest (up to $\simeq m_\phi$). It is shown in [63] that a first degree polynomial $K(s) = 1 + \alpha_\Omega s$ allows to reach a nice (linear) correlation up to $s \simeq 1 \text{ GeV}^2$ between the dipion spectrum from Belle [23] and the $\Omega(s)$ functions derived from the phase shift data from [67]; a value $\alpha_\Omega \simeq 0.1 \text{ GeV}^{-2}$ can be inferred from Figure 1 in [63]. The deterioration of the linear behavior above $s \simeq m_\phi^2$ is, actually, not unexpected because of rising inelasticities and of the high mass vector meson influence.

ii) Assuming the pion pair emerging from the η/η' radiative decays is purely Isospin 1 and P -wave [56, 53], its amplitude should carry the same analytic properties than $F_\pi(s)$, *i.e.* they may only differ by a real-analytic function, free of right-hand side singularities. Reference [62] thus proposes to write the differential dipion spectra :

$$\frac{d\bar{\Gamma}_X}{ds} = \Gamma_0(s) |A_X P_X(s) F_\pi(s)|^2 \text{ , } (X = \eta/\eta') \text{ ,} \quad (30)$$

where $\Gamma_0(s)$ has been already defined in Equations (26) and the A_X 's being appropriate normalization constants. The $P_X(s)$ functions ($P_X(0) = 1$) are remaining correction factors specific of the η and η' radiative decays which could both be analyzed within the Extended ChPT context [35, 37] (see also [68]) and are free of right-hand side singularities.

As just argued regarding the pion form factor and its $K(s)$ factor, the $P_X(s)$ functions should satisfactorily be approximated by low degree polynomials [62]. This is what is shown by the downmost panel in Figure 1 of [63] which, moreover, indicates that $P_\eta(s) = P_{\eta'}(s)$ should likely hold. Of course, procedures to complement this approach by symmetry breaking effects have also to be invoked, prominently the $\rho^0 - \omega$ mixing for the η' decay process – but not only.

iii) The issue is now to relate $d\bar{\Gamma}_X$ (Equation (30)) and $d\tilde{\Gamma}_X$ (Equation (26)) within the HLS framework *when no breaking is at work*. Equivalently, this turns out to check whether the $R_X(s)$'s and $F_\pi(s)$ (can) carry the same phase in this case.

Let us consider the pion vector form factor $F_\pi(s)$ as given in [17], discarding terms of order $\mathcal{O}(\delta)$ or higher in breaking parameters; keeping only tree contributions (loop corrections, like the $\rho^0 - \gamma$ transition amplitude, are counted as $\mathcal{O}(\delta)$) and dropping out the \mathcal{L}_{p^4} contributions, one derives ($m^2 = ag^2 f_\pi^2$, the unbroken ρ^0 HK mass) :

$$F_\pi(s) = \left(1 - \frac{a}{2} \left[1 + \frac{m^2}{D_\rho(s)} \right] \right) + \mathcal{O}(\delta) . \quad (31)$$

Similarly, the $R_X(s)$ functions in Equation (26) reduce to :

$$R_\eta = -\frac{ie \sin \delta_P}{4\pi^2 f_\pi^3} \left(1 - \frac{3}{2} c_3 \left[1 + \frac{m^2}{D_\rho(s)} \right] \right) , \quad R_{\eta'} = +\frac{ie \cos \delta_P}{4\pi^2 f_\pi^3} \left(1 - \frac{3}{2} c_3 \left[1 + \frac{m^2}{D_\rho(s)} \right] \right) \quad (32)$$

up to terms of $\mathcal{O}(\delta)$ in breaking parameters,

These Equations lead us to define a *no-breaking* reference by requiring :

1/ The holding of the Vector Meson Dominance assumption which implies $a \equiv a_{VMD} = 2$ within the generic HLS model [9, 13]. It is worthwhile reminding here (see Section 2 in [18] for details) that the HLS parameter a is not reachable by fit, once the BKY breaking (see Appendix A.2) is at work; indeed, all Lagrangian terms of interest for our physics depend on the product $a' = a(1 + \Sigma_V)$ and not on each of these parameters separately; therefore one can freely fix $a = 2$ and, then, the term $\delta a = a_{VMD} \Sigma_V$ is clearly⁸ $\mathcal{O}(\delta)$.

2/ The universality of the ρ phase implies that $R_\eta(s)$, $R_{\eta'}(s)$ and $F_\pi(s)$ share the same phase and, therefore, it requires the existence of an "unbroken" value for c_3 : Indeed, imposing $c_3^{ref} = 2/3$ beside $a_{VMD} = 2$, one can derive a satisfactory no-breaking reference as, one obtains :

$$F_\pi(s) = -\frac{m^2}{D_\rho(s)} \quad R_\eta = +\frac{ie \sin \delta_P}{4\pi^2 f_\pi^3} \frac{m^2}{D_\rho(s)} , \quad R_{\eta'} = -\frac{ie \cos \delta_P}{4\pi^2 f_\pi^3} \frac{m^2}{D_\rho(s)} . \quad (33)$$

which should be complemented by $\mathcal{O}(\delta)$ contributions to account for real data.

The issue becomes whether the values returned for a and c_3 from fits to the (real) data differ little enough from a_{VMD} and c_3^{ref} that their differences can be considered $\mathcal{O}(\delta)$ effects. For this purpose, one can refer to the latest published BHLS₂ standard fit results collected in Table 10 of [18], in particular, one finds :

- $a = 1.766 \pm 0.001$ which shows a deviation $\delta a = 0.244$ from $a_{VMD} = 2$ corresponding to having $\Sigma_V = 0.122$,
- $c_3 = 0.742 \pm 0.003$ which deviates by $\delta c_3 = 0.076$ from $c_3^{ref} = 0.667$,

focusing on the favored solution A_- [18] to the Kroll conditions (see Section 3) – the A_+ solution actually provides similar values. Thus, δa and δc_3 look small enough to be viewed

⁸In the course of the fitting procedure, it is as appropriate to either choose fitting a , fixing $\Sigma_V = 0$ or fix a and fit Σ_V ; we choosed the first option.

as departures from resp. a_{VMD} and c_3^{ref} and treated as $\mathcal{O}(\delta)$ corrections, on the same footing than the manifest breaking parameters. To our knowledge, it is the first time that an identified physics condition can propose a constraint on one of the FKTUY [10] parameters, namely⁹ c_3 .

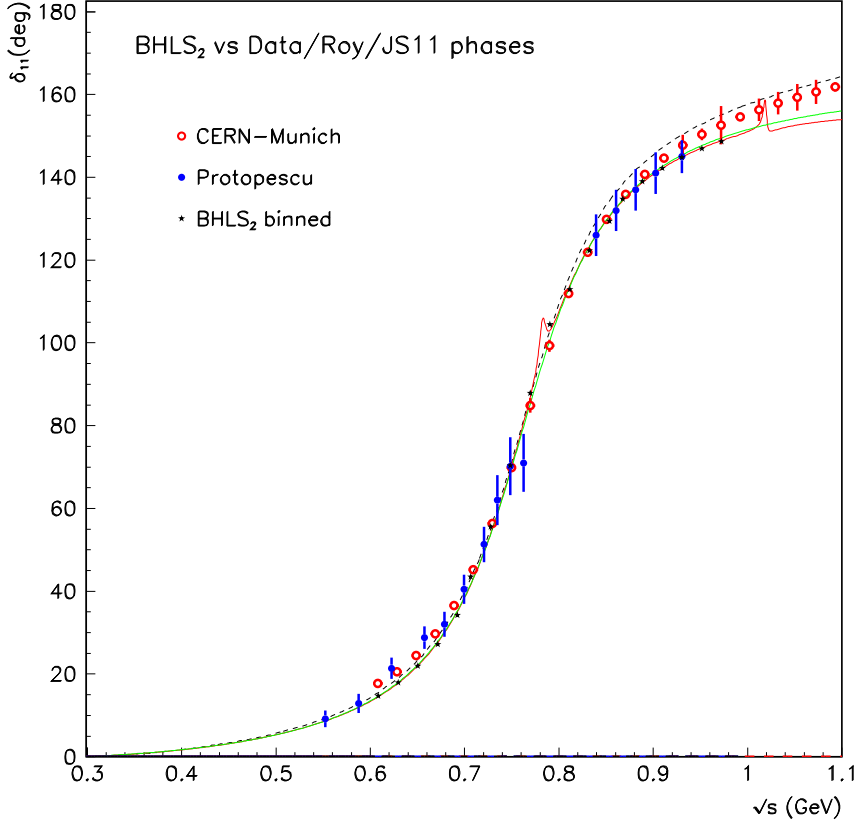


Figure 2: The δ_{11} phase-shift plotted as function of \sqrt{s} . Beside the data points of [69, 70], the dashed black curve is the solution to the Roy Equations [71], the green full line shows the phase reconstructed in [72] and red full line the BHLS₂ phase-shift exhibiting the ω and ϕ signals. The black stars show the smeared BHLS₂ spectrum (e.g. the red curve).

iv) From what has been just argued, it is clear that, within the BHLS₂ context, the $\eta/\eta' \rightarrow \pi^+\pi^-\gamma$ decay amplitudes $T_X(s)$ reported in Sections 5 and 6 above can actually be written :

$$T_X(s) = B_X F_\pi(s) + \mathcal{O}(\delta) \quad , \quad X = \eta/\eta' \quad , \quad (34)$$

⁹Actually, another condition comes out from the data in analyses performed within the HLS context : $c_3 = c_4$.

the B_X 's being definite constants depending on the breaking parameters. $F_\pi(s)$ contains already manifest breaking terms like the ω and ϕ signals with, however, different weights from their analogs in the $T_X(s)$ amplitudes¹⁰.

On the other hand, as shown in [17], yielding a fair description of the data samples for $|F_\pi(s)|$ (see Figure 2 and Table 3 in [17]), BHLS₂ also leads to a fair account of the phase-shift $\delta_{11}(s)$ over its whole range of validity *without involving any phase-shift data sample in its derivation*. This is illustrated by¹¹ Figure 2 which reflects the fair accord reached by the BHLS₂ prediction with the phase derived from the Roy Equations [71] or the pion form factor phase of Reference [72] on the one hand, and the experimental phase shift data from [69, 70] on the other hand. Moreover, the same BHLS₂ spectrum smeared over 10 MeV bins – to mimic the Cern-Munich spectrum [69] – (black star symbols) clearly shows that the ω and ϕ signals cannot be manifestly observed in the existing data.

All this leads to conclude that the SHKMW modification [62] shown in Equation (30) :

$$F_\pi(s) \rightarrow A_X P_X(s) F_\pi(s)$$

to account for the Final State Interaction (FSI) among the pions emerging from the radiative η/η' decays also applies in the global BHLS₂ context. In this case, this turns out to perform the change :

$$T_X(s) \implies H_X P_X(s) T_X(s)$$

when using the amplitudes constructed in Sections 5 and 6. Our notations are connected with those in Reference [62] by writing these¹² :

$$A_X = A_X^0 H_X \quad , \quad H_X \equiv 1 + \delta_X \quad , \quad X = \eta, \eta' \quad (35)$$

as the A_X^0 factors are already accounted for in the T_X amplitudes derived from the BHLS₂ Lagrangian as shown below.

Then, the global character of the BHLS₂ fitting context¹³, ensures that the non-perturbative effects are suitably accounted for as reflected by Figure 2. Figure 3 sketches the procedure which will be followed.

From now on, the $P_X(s)$ functions are chosen polynomials of the lowest possible degree consistent with a satisfactory fitting. Being beyond the BHLS₂ scope, these functions are supplemented within the fit procedure by performing the change :

$$T_X(s) \implies H_X P_X(s) T_X(s) \quad , \quad \text{with } P_X(0) = 1 \quad , \quad X = \eta, \eta' \quad (36)$$

in Equation (25) above. Practically, each term in the right-hand side of Equation (25) gets a factor of $|H_X P_X(s)|^2$, the coefficients of which having to be derived by the global fit where the $[C_X]^2$ term can be discarded as it is manifestly $\mathcal{O}(\delta^2)$.

¹⁰For instance, BHLS₂ predicts that the coupling ratio $\omega\pi\pi$ to $\rho^0\pi\pi$ is 3 times smaller in the η' radiative decay than in the pion vector form factor.

¹¹Reprinted from Figure 10 in [17].

¹²Actually, to be formally exact, Reference [62] writes $A = A_0(1 + \delta)$ for the η meson decay, and $A' = A'_0(1 + \delta')$ for the η' meson, as can be read around their Relations (9).

¹³In this case, its Reference set of data samples \mathcal{H}_R [17, 18], which already includes most of the existing pion form factor data samples will be supplemented with the η/η' dipion spectra.

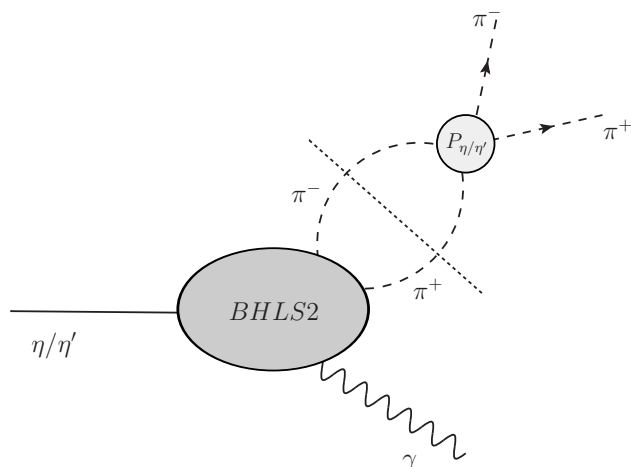


Figure 3: Diagram sketching the sharing between $BHLS_2$ and the Final State Interaction process in the η/η' decays to $\pi^+\pi^-\gamma$. In the global fit context, $T_X(s)$, represented by the lower blob, takes care of the non-perturbative effects. The drawing somewhat anticipates about the $P_X(s)$ universality.

10 Fits of the η/η' Radiative Decay Spectra within $BHLS_2$

The reference set of data samples \mathcal{H}_R included within the $BHLS_2$ framework has been presented several times and recently in [17, 18]; it covers the six e^+e^- annihilation channels to $\pi^+\pi^-$, K^+K^- , K_LK_S , $\pi^+\pi^-\pi^0$, $\pi^0\gamma$, $\eta\gamma$, some more decay widths (in particular $\pi^0/\eta/\eta' \rightarrow \gamma\gamma$) and, finally, the dipion mass spectrum in the $\tau \rightarrow \pi\pi\nu$ decay. These represent already the largest set of data (altogether 1366 data points) successfully submitted to a global fit, as reflected by Table 9 in [18]; they will not be discussed here any more. It is nevertheless relevant to remind that \mathcal{H}_R encompasses almost all existing samples except for the recent CMD-3 dipion data as already argued in footnote ³, the KLOE08 [32], Babar [30, 31] and the recent SND [73] dipion spectra because of the strong tension they exhibit with respect to the rest of the (more than 60) \mathcal{H}_R samples. This issue has been thoroughly reexamined in [18].

The present study aims at including also the dipion spectra measured in the η/η' radiative decays within the global $BHLS_2$ framework. However, it is certainly cautious to avoid using *simultaneously* the η/η' dipion spectra and the $\pi^+\pi^-\pi^0$ annihilation data within global fits as long as a specific study has not assessed some clear statement about FSI in the latter channel¹⁴ and data.

On the other hand, it is worthwhile to stress that all the published dipion spectra of the $\eta/\eta' \rightarrow \pi^+\pi^-\gamma$ decays carry an arbitrary normalization; so, it is important to stress that *they*

¹⁴The fit results reported in [17, 18] may as well indicate that FSI effects are small or effectively absorbed in the parameter values returned by the fits. Anyway, this certainly deserves a devoted work [74].

only provide the spectrum lineshapes measured by the various experiments. It follows from this peculiarity that they allow to fit *only* the $P_X(s)$ polynomials and they are totally insensitive to the H_X parameter values; this issue will be addressed by performing global fits where the corresponding partial widths – taken from the Review of Particle Properties (RPP) [59] – are also considered inside the fitting procedure.

10.1 Available Dipion Spectra from the $\eta/\eta' \rightarrow \pi^+\pi^-\gamma$ Decays

Measurements of the dipion spectrum in the $\eta' \rightarrow \pi^+\pi^-\gamma$ decay started long ago – as early as 1975 [41] – and several experiments have collected samples of various (but low) statistics motivated by the $\simeq 20$ MeV shift reported for the ρ^0 peak location compared to its value in $e^+e^- \rightarrow \pi^+\pi^-$ annihilations : JADE [42], CELLO [43], TASSO [44], PLUTO [45], TPC-2 γ [46], ARGUS [47], Lepton F [48]; the Crystal Barrel Collaboration published by 1997 the most precise spectrum [49] carrying 7400 events. The breakthrough has come from the BESIII Collaboration [53] which published a 970,000 event spectrum by 2017.

The formerly collected samples have been examined and their behavior is briefly reported below. Dealing with the uncertainty information provided with these η' samples is generally straightforward, except for the BESIII dipion spectrum [53] for which a spectrum for the energy resolution is provided. It is accounted for by replacing within the minimization procedure the genuine model function value by that of its convolution with the resolution function, assuming the provided resolutions be the standard deviations of gaussians; the net effect of the BESIII energy resolution information deserves to be shown (see below).

The BESIII data [57] are provided as two 112 data point spectra, the former giving the numbers of η' event candidates in 10 MeV bins (N_{evt}^i), the latter the estimated numbers of background events (N_{bkg}^i) within the same bins. One has provided our global fitting code with the $N_{signal}^i = N_{evt}^i - N_{bkg}^i$ spectrum; we have assumed the original distributions poissonian and fully correlated by attributing to N_{signal}^i an uncertainty $\sigma_i = \sqrt{N_{evt}^i} + \sqrt{N_{bkg}^i}$; it is shown below that these specific assumptions allow a fair dealing with the BESIII spectrum [53].

On the other hand, the reported dipion spectrum observed in the parent $\eta \rightarrow \pi^+\pi^-\gamma$ decay has undergone much less measurements. Beside former spectra¹⁵ from Layter *et al.* [54] and Gormley *et al.* [55], WASA-at-COSY reported for a 14,000 event spectrum [56] whereas the KLOE/KLOE2 Collaboration has collected a 205,000 event spectrum [57]; it should be noted that the WASA dipion spectrum is given with only statistical errors.

It is worth stressing again that the normalization of all these spectra being arbitrary, the theoretical (absolute) distribution scales provided by the BHLS₂ Lagrangian are lost when normalizing to the specific scale of each data set when fitting; stated otherwise these data samples only allow to address the fit of the $P_X(s)$ functions ($X = \eta, \eta'$) and *not* of the H_X constants which are cancelled out when normalizing the model functions to the experimental spectra.

¹⁵The numerical content of these spectra can only be derived from the paper Figures.

10.2 η/η' Experimental Spectra : Fits in Isolation

The first exercise is thus to explore the degree issue for the $P_X(s)$ polynomials and so, does not need to deal with complications due to keeping the constant H_X within the fit procedure. Therefore, fits have been performed, supplementing the Reference data set of samples \mathcal{H}_R by either of the experimental η' or η spectra. In this Section, one only reports on using the A_- BHLS₂ variant¹⁶ [18] which will be our working BHLS₂ version.

Regarding the $P_{\eta'}(s)$ polynomial, the results given in the Table just below¹⁷ focus on only the BESIII η' sample (112 data points) [53]; indeed, because of their statistics, all the other η' dipion spectra, including the Crystal Barrel one [49], do not exhibit any clear sensitivity to the $P_{\eta'}$ degree and may easily accomodate $P_{\eta'} \equiv 1$.

$P_{\eta'}(s)$ degree	1	2	3
$\chi^2_{BESIII} (N = 112)$	160	99	98
$\chi^2_{TOT} (N = 1187)$	1167	1097	1096
Probability	44.7%	90.6%	90.8 %

This clearly points out that, thanks to the statistics reached by the BESIII Collaboration, the first degree for $P_{\eta'}(s)$ can be excluded ($\langle \chi^2 \rangle = 1.43$) and the third degree is obviously useless.

Regarding the η data, complementing \mathcal{H}_R with the KLOE/KLOE2 sample (59 data points) [57] alone or together with the WASA one (37 data points) [56], the picture returned by the fits is much less conclusive as a first degree $P_{\eta}(s)$ provides¹⁸ $\chi^2(KLOE/KLOE2) = 55$ and $\chi^2(WASA) = 45$, and a second degree $P_{\eta}(s)$ yields $\chi^2(KLOE) = 51$ and $\chi^2(WASA) = 51$ with similar fit probabilities, both at the 90% level, as just above. The choice of minimal degree has been preferred for $P_{\eta}(s)$.

Therefore, in the following, when different, the polynomials $P_{\eta}(s)$ and $P_{\eta'}(s)$, are definitely chosen, the former first degree, the latter second degree. The polynomial coefficients returned by the global fits performed with the A_- BHLS₂ variant are discussed below and given in Table 2.

It is worthwhile noting that the degradation of the fit quality observed when assuming a first degree $P_{\eta'}(s)$ is essentially carried by the the BESIII $\eta'(s)$ data sample itself, with a quite marginal influence on the standard channels of the BHLS₂ framework and on the η dipion spectra. This emphasizes the robustness of the BHLS₂ Lagrangian.

In order to lighten the forthcoming discussion, let us comment right now on the formerly

¹⁶Nevertheless, the most relevant results obtained using the A_+ BHLS₂ variant are summarized in the following Subsections.

¹⁷The fits which provide these results have been performed with our Reference set amputated from the $e^+e^- \rightarrow \pi^+\pi^-\pi^0$ annihilation data. The number of BESIII data points and the total number of fitted data points are given by the N values within parentheses.

¹⁸Note that $\chi^2(WASA)$ is always overestimated because of an incomplete reported experimental error information.

collected (η/η') dipion spectra listed in the Subsection above which have also been analyzed within the BHLS₂ context; they quite generally yield stable χ^2/N values. Some of them return large χ^2/N values from the global fit procedure, namely, those from TPC-2 γ (69/13), LEPTON-F (45/20) and Layter *et al.* (60/15). Most of these former samples, however, are getting reasonable χ^2/N values, typically 8/12 (TASSO), 15/21 (CELLO), 23/18 (PLUTO), 20/15 (ARGUS), 11/17 (CRYSTAL BARREL¹⁹), 13/14 (Gormley *et al.*) but have a quite negligible impact on the issues examined in the present study. Therefore one focuses on the high statistics data samples from BESIII and KLOE/ KLOE2; the case for the WASA data set may be nevertheless commented¹⁸.

10.3 The η/η' Experimental Spectra : Analysis within the BHLS₂ Context

Table 1 collects the relevant fit quality information derived when running global fits within the A_- BHLS₂ variant. The first data column gives the fit information in a global fit performed²⁰ by discarding the η/η' to provide the BHLS₂ reference fit pattern; using the full \mathcal{H}_R , one would have found the numbers given in the last data column of Table 9 in [18]. The second and third data columns report on the fits performed by including η/η' dipion spectra within the fit data set \mathcal{H}_R under the conditions indicated in the top line of Table 1.

The fit information concerning the $e^+e^- \rightarrow \pi^+\pi^-$ annihilation data collected in scan mode (with different detectors at the various Novosibirsk facilities) is displayed in the first data line (the exact sample content behind the wording NSK is explained in [18], for instance). The line KLOE stands for the merging of the KLOE10 [27] and KLOE12 [28] data samples. The spacelike pion form factor data merges the NA7 and Fermilab samples [76, 77].

Taking the first data column of Table 1 as reference, one can clearly conclude that the fit quality obtained when using the η/η' dipion spectra is unchanged and fairly good. Indeed, the χ^2 increase of the NSK set of scan data samples is obviously negligible and those of the ISR data collected under the name KLOE and spacelike data are unchanged. The description of the data samples in the other channels from BHLS₂ (not shown) is also unchanged²¹.

Regarding the Triangle Anomaly sector, the χ^2 information for the $\pi^0/\eta/\eta' \rightarrow \gamma\gamma$ decays are :

$$\left\{ \begin{array}{l} \text{BHLS}_2 \text{ } A_- \text{ variant with } P_\eta(s) \neq P_{\eta'}(s) : (\chi_{\pi^0}^2, \chi_\eta^2, \chi_{\eta'}^2) = (1.08, 0.01, 3, 33) \\ \text{BHLS}_2 \text{ } A_- \text{ variant with } P_\eta(s) \equiv P_{\eta'}(s) : (\chi_{\pi^0}^2, \chi_\eta^2, \chi_{\eta'}^2) = (0.73, 0.03, 4.77) \end{array} \right. \quad (37)$$

Thus, the RPP width [59] for $\pi^0 \rightarrow \gamma\gamma$ is reproduced at the $(0.9 \div 1)$ σ level and the one for $\eta \rightarrow \gamma\gamma$ is reconstructed at nearly its RPP value; the width for $\eta' \rightarrow \gamma\gamma$ is found in the range $(1.8 \div 2.2)$ σ , somewhat larger but still acceptable.

On the other hand and more importantly : Comparing the second and third data columns of Table 1 obviously substantiates the SHKMW conjecture [62] about the universality of the

¹⁹Its data point at 812.5 MeV, soon identified as outlier, being dropped out; see footnote 21 in [75].

²⁰ The $e^+e^- \rightarrow \pi^+\pi^-\pi^0$ annihilation data are switched off.

²¹Their variations are always χ^2 unit fractions.

χ^2/N_{pts} Fit Configuration (A_-)	no η/η' Spectra	$P_\eta(s) \neq P_{\eta'}(s)$	$P_\eta(s) \equiv P_{\eta'}(s)$
NSK $\pi^+\pi^-$ (127)	137/127	139/127	140/127
KLOE $\pi^+\pi^-$ (135)	141/135	140/135	140/135
Spacelike $\pi^+\pi^-$ (59)	64/59	64/59	64/59
η' BESIII (112)	×	100/112	102/112
η KLOE/KLOE2 (59)	×	57/59	55/59
Total χ^2/N_{pts}	995/1075	1156/1246	1154/1246
Fit Probability	88.6 %	89.7%	90.6%

Table 1: Fit properties of selected dipion data sample sets using the A_- BHLS₂ variant. The fit reported in the first data column is free of η/η' dipion influence. The second data column corresponds to fitting with independent $P_\eta(s)$ and $P_{\eta'}(s)$, whereas the third data column reports on the fit where $P_\eta(s) \equiv P_{\eta'}(s)$ has been imposed. The χ^2/N_{pts} value for the WASA sample, fitted or not, is in the range¹⁸ (44 – 47) for 37 data points.

$P_X(s)$ function, e.g. $P_\eta(s) \equiv P_{\eta'}(s)$. One may also note the slight improvement generated by having stated $P_\eta(s) \equiv P_{\eta'}(s)$; this should be due to having provided its curvature to $P_\eta(s)$ which in turn lessens the (already marginal) tension between the KLOE/KLOE2 and BESIII data samples.

Before going on with solely using the A_- variant of the BHLS₂ Lagrangian, it is worthwhile reporting on its A_+ variant behavior. Let us limit oneself to reporting on the A_+ variant best fit performed assuming $P_\eta(s) \equiv P_{\eta'}(s)$ second degree; one obtains $\chi^2/N(\text{BESIII}) = 110/112$, and the η dipion spectrum from the KLOE/KLOE2 Collaboration yields this ratio at 54/59; for its part, the unfitted WASA sample yields 49/37. The global fit probability is 51.5% only, to be compared to 90.6 % for the global fit performed under the A_- variant reported in Table 1.

This drop in probability is noticeable and its reason deserves to be identified; indeed, the $\chi^2(\text{BESIII})$ increases by "only" 8 units, whereas the χ^2 for the η dipion spectra are almost unchanged compared to Table 1. Moreover, the usual BHLS₂ channels also benefit from χ^2 's comparable in magnitude to their A_- analogs. Surprisingly, the single place where the disagreement blows up is in the $\gamma\gamma$ decays as :

$$(\chi_{\pi^0}^2, \chi_\eta^2, \chi_{\eta'}^2) = (29.92, 0.34, 0.08) \quad ,$$

e.g. the $\pi^0 \rightarrow \gamma\gamma$ partial width is at more than 5σ from its accepted value [59], which is by far too large to be acceptable. Indeed, this implies that the A_+ fit central value for the $\pi^0 \rightarrow \gamma\gamma$ partial width is reconstructed at 70% of its present RPP value [59]; this should be brought in

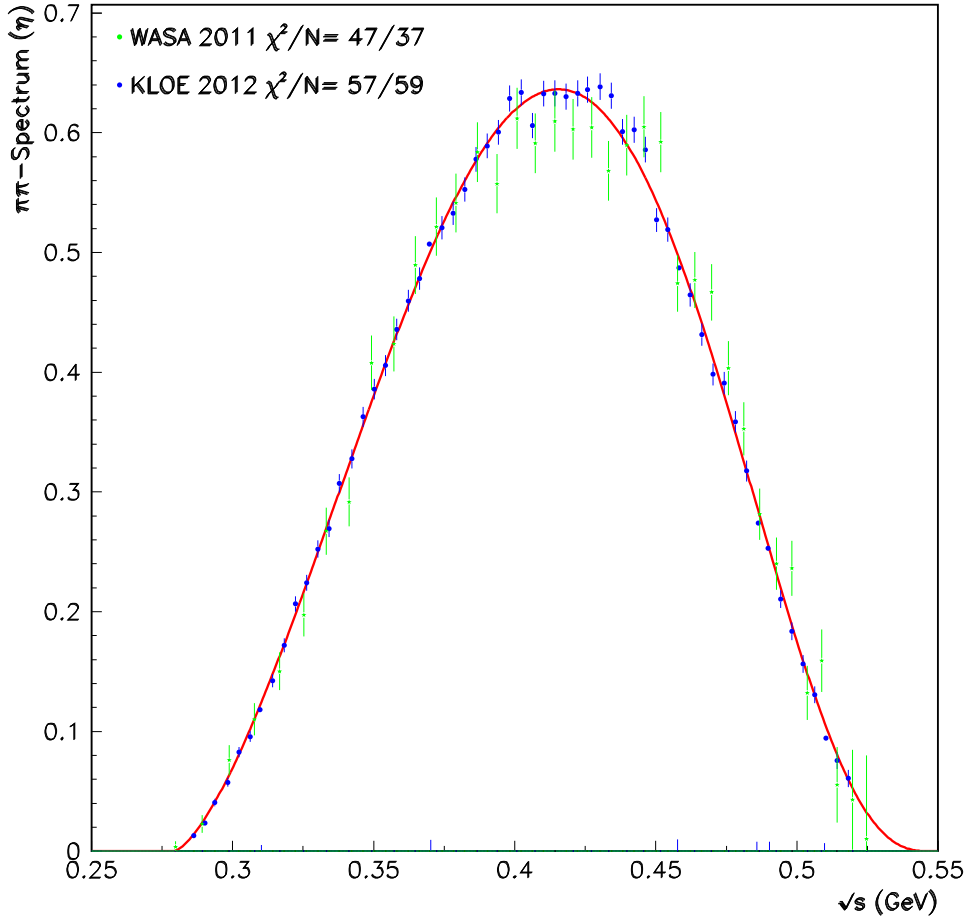


Figure 4: The dipion invariant mass spectrum in the $\eta \rightarrow \pi^+\pi^-\gamma$ decay. The blue data points are the KLOE/KLOE2 spectrum, the green ones display the WASA spectrum. The red curve is the BHLS₂ fit leaving free the $P_\eta(s)$ polynomial. Vertical units are arbitrary.

balance with the A_- variant which yields this partial width reconstructed 5% larger from the expected value (7.8 eV).

Therefore, the A_+ variant unexpectedly exhibits a strong tension between the Triangle and Box Anomaly sectors of the BHLS₂ Lagrangian, whereas the A_- variant behaves smoothly in both sectors. Therefore, from now on, one will focus on the A_- variant of BHLS₂ which becomes our Reference model; results derived using the A_+ variant are no longer reported *except when explicitly stated*.

Regarding the η spectra, Figure 4 shows an almost perfect account of the KLOE/KLOE2 spectrum : the BHLS₂ spectrum matches the dipion spectrum from KLOE/KLOE2 [57] on the whole energy range, except for a marginal issue in the 0.45 GeV energy region. Even if its χ^2 value is acceptable, the WASA spectrum [56] may look somewhat distorted with respect to its KLOE/KLOE2 partner, clearly favored by BHLS₂ expectations¹⁸.

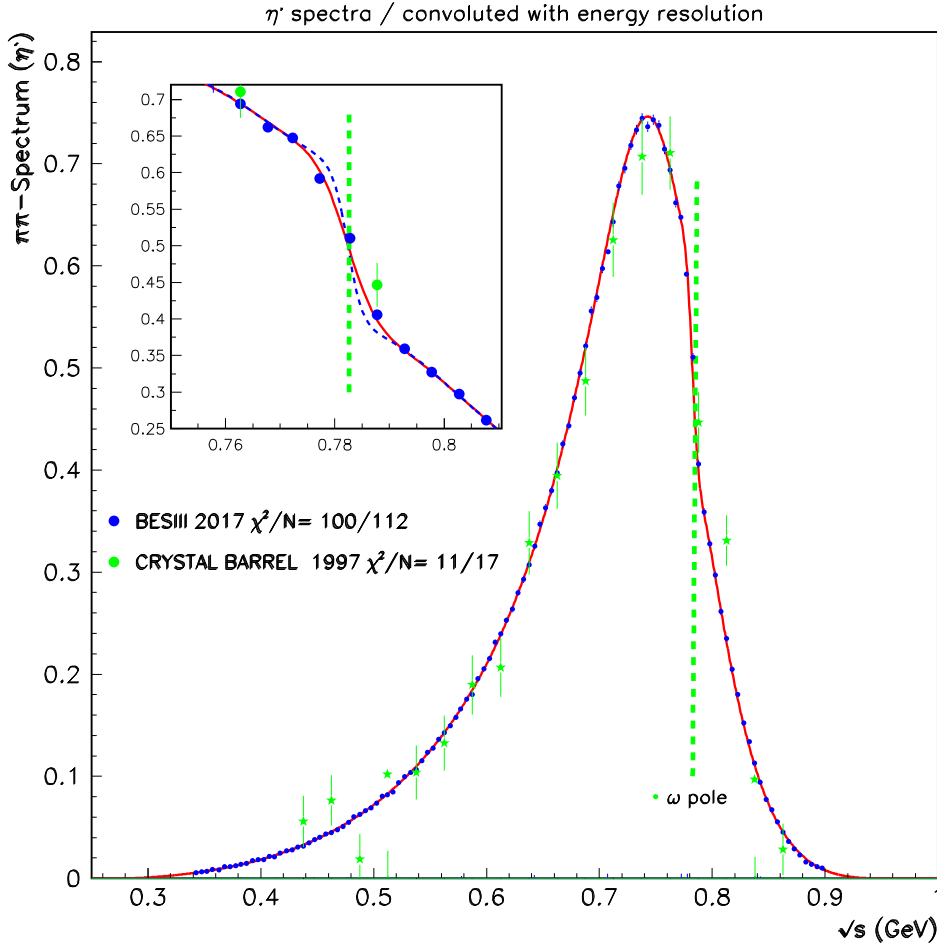


Figure 5: The dipion invariant mass spectrum in the $\eta' \rightarrow \pi^+\pi^-\gamma$ decay. The blue data points are the BESIII spectrum, the green ones are those from Crystal Barrel. The red curve is the fit function, *i.e.* the convolution of the BHLS₂ model function with the energy resolution function assumed gaussian; the blue curve is the underlying BHLS₂ model function itself. Both curves superimpose over the whole energy range except for the $\rho - \omega$ drop-off region. Vertical units are arbitrary.

Regarding the η' spectrum, Figure 5 shows a noticeably fair accord between the BHLS₂ modeling and the BESIII spectrum [53] all along the energy range. The vertical green dotted lines locate the ω mass and so the ρ – ω drop–off region, otherwise magnified in the inset. Here, one can observe the effect of convoluting the BHLS₂ model function with energy resolution gaussians as provided by the BESIII Collaboration : It does perfectly what it is supposed to do, *i.e.* soften the drop–off to its right lineshape with, moreover, a noticeable accuracy. On the rest of the spectrum, the convoluted curve and the underlying model one superimpose on each other within the thickness of the curves. One should also state that no tension in the ρ – ω drop–off region is observed in the fits with any of the other dipion spectra submitted to the fit.

It is useful to consider the spectra²² :

$$\overline{P}_X(s) = \left[\frac{d\Gamma_{exp}(s)}{d\sqrt{s}} / \frac{d\Gamma_{theor}(s)}{d\sqrt{s}} \right]_X P_X(s) , \quad X = \eta, \eta' \quad (38)$$

to illustrate the behavior of the $P_X(s)$ polynomials under the two assumptions discussed above. As the bracketed term in Equation (38) fluctuates around 1 and reflects the experimental uncertainty spectrum, the $\overline{P}_X(s)$ spectrum looks an appropriate experimentally based evaluation of its corresponding model function $P_X(s)$.

Figure 6 displays the $\overline{P}_{\eta'}(s)$ and $\overline{P}_\eta(s)$ spectra defined just above in the case of BESIII, KLOE/KLOE2 and WASA spectra together with their model partners $P_{\eta'}(s)$ (second degree) and $P_\eta(s)$ (first degree). As could be inferred from the fit properties shown in Table 1, $P_{\eta'}(s)$ (the red dashed curve in the inset) is also a good evaluation for $\overline{P}_\eta(s)$.

Figure 7 also displays the $\overline{P}_{\eta'}(s)$ and $\overline{P}_\eta(s)$ spectra for the BESIII, KLOE/KLOE2 and WASA data samples, but together with their common model fit function denoted $P_X(s)$, a second degree polynomial. As reflected by the fit information reminded in the body of the Figure, one has reached a fair simultaneous parametrization of the η and η' dipion spectra by only supplying the BHLS₂ model amplitudes with a single second degree polynomial $P_X(s)$ fulfilling $P_X(0) = 1$.

10.4 Final State Interaction: BHLS₂ Fit Results versus Others

The top bunch in Table 2 displays the values returned for the polynomial coefficients of :

$$P_\eta(s) = 1 + \alpha_1 s \quad \text{and} \quad P_{\eta'}(s) = 1 + \alpha'_1 s + \alpha'_2 s^2 . \quad (39)$$

When using the same polynomial for the η and η' spectra, it is second degree and denoted $P_X(s)$. It should be noted that the coefficients for $P_{\eta'}(s)$ (second data column) and $P_X(s)$ (third data column) carry numerical values close to each other, *i.e.* at $\simeq 1 \sigma$ from each other for both the first and second degree coefficients²³. In the case of having a (single) common FSI function $P_X(s)$, the covariance is $\langle \delta\alpha'_1 \delta\alpha'_2 \rangle = -0.746$.

²²It is, of course, understood that, when dealing with the BESIII η' dipion sample, $d\Gamma_{theor}(s)/d\sqrt{s}$ is, actually, the convolution product of the model function with the BESIII energy resolution function.

²³It might be useful to provide, for completeness, the covariances when $P_\eta(s) \neq P_{\eta'}(s)$: Using obvious notations, they are $\langle \delta\alpha_1 \delta\alpha'_1 \rangle = -0.005$, $\langle \delta\alpha_1 \delta\alpha'_2 \rangle = -0.026$ and $\langle \delta\alpha'_1 \delta\alpha'_2 \rangle = -0.812$.

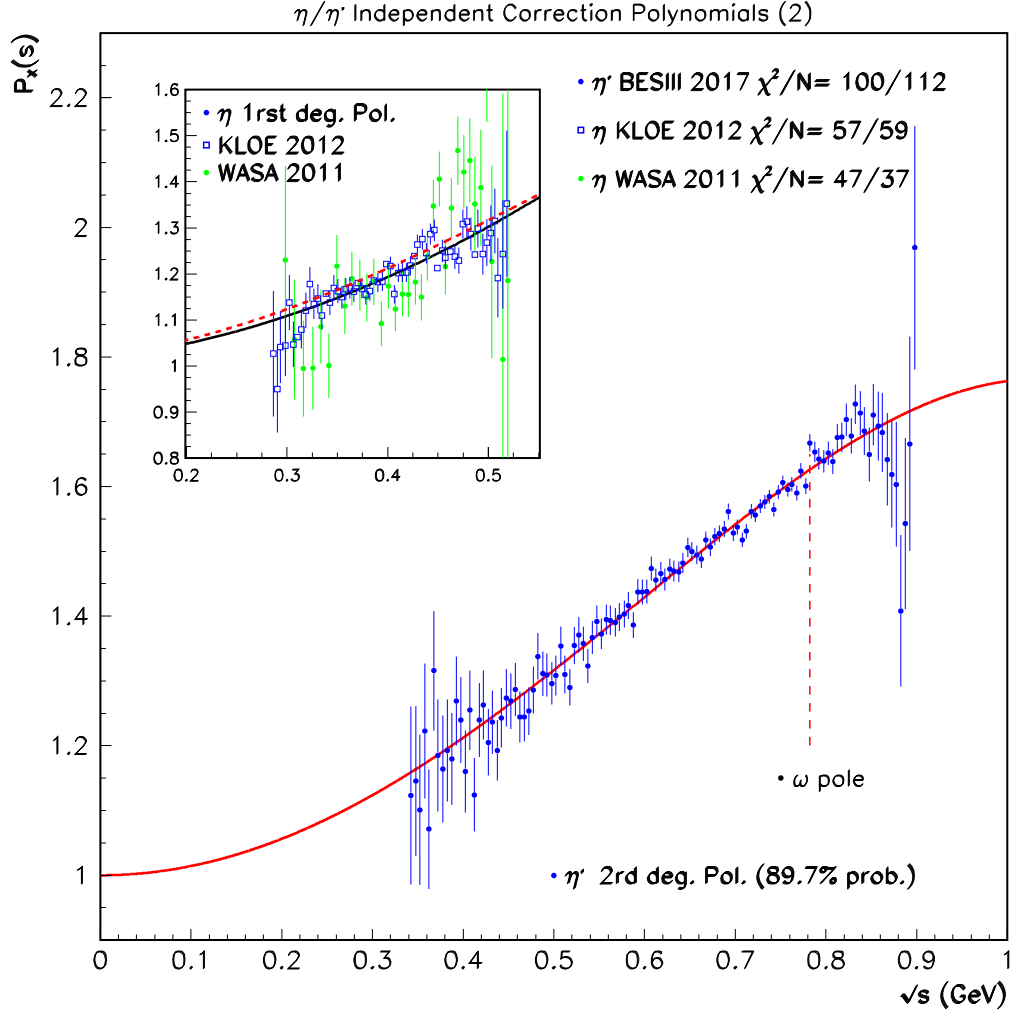


Figure 6: The $\overline{P}_{\eta'}(s)$ and, in the inset, the $\overline{P}_{\eta}(s)$ spectra (Equation (38)). The full red curve and full black curve superimposed to resp. $\overline{P}_{\eta'}(s)$ and $\overline{P}_{\eta}(s)$ are resp. the $P_{\eta'}(s)$ and $P_{\eta}(s)$ polynomials returned by the fits. The dashed red curve in the inset is also $P_{\eta'}(s)$, but superimposed to the $\overline{P}_{\eta}(s)$ spectrum. Some pieces of fit information are also displayed.

Regarding the systematics : In the BHLS₂ approach, the statistical and systematic uncertainties provided by the experiments together with their spectra are carefully embodied within the fitting code without any modification; so our reported uncertainties automatically merge both kinds of experimental errors. On the other hand, the last two data lines in Table 2 clearly illustrate that $\delta a = a - 2$ and $\delta c_3 = c_3 - 2/3$ remain consistent with expectations, *i.e.* they can

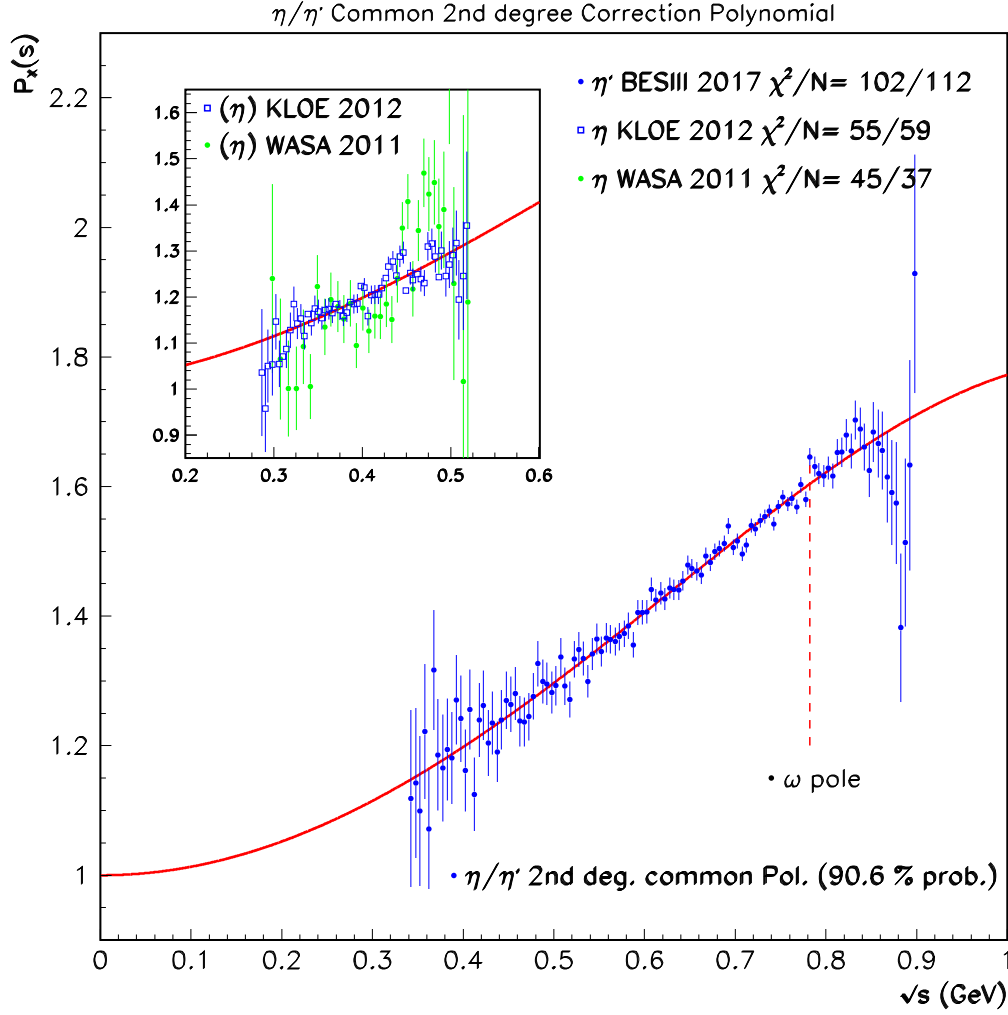


Figure 7: The $\overline{P}_{\eta'}(s)$ and, in the inset, the $\overline{P}_{\eta}(s)$ spectra (Equation (38)). The full red curve superimposed on the $\overline{P}_{\eta'}(s)$ and, in the inset, the $\overline{P}_{\eta}(s)$ spectra is their common fit function $P_X(s)$. The ω pole location is indicated. Some pieces of fit information are also displayed.

be regarded as $\mathcal{O}(\delta)$ breaking parameters. The other fit parameter values are given in Table 5 displayed in Appendix E; they are scrutinized in order to detect some hint regarding the FSI effects in the 3π channel of the BHLS₂ model – where they are not implemented by now.

- **j/** Regarding the $P_{\eta}(s)$ FSI polynomial, it is worth comparing our numerical value for α_1 with those available in the literature. The first published evaluation (GeV^{-2}) of α_1 is the

Fit Parameter Value	no η/η'	$P_\eta(s) \neq P_{\eta'}(s)$	$[A_-] : P_X(s)$	$[A_+] : P_X(s)$
α'_1 (GeV ⁻²)	×	1.388 ± 0.072	1.326 ± 0.053	0.953 ± 0.065
α'_2 (GeV ⁻⁴)	×	-0.607 ± 0.055	-0.553 ± 0.048	-0.511 ± 0.052
α_1 (GeV ⁻²)	×	1.169 ± 0.063	×	×
a_{HLS}	1.789 ± 0.001	1.842 ± 0.001	1.821 ± 0.001	1.830 ± 0.001
$(c_3 + c_4)/2$	0.756 ± 0.005	0.773 ± 0.005	0.772 ± 0.004	0.819 ± 0.007
Fit Probability	88.6 %	89.7%	90.6%	51.4%

Table 2: The FSI parameter values from the A_- BHLS₂ variant fit. the first data column reports on the fit performed by submitting the usual set of data samples \mathcal{H}_R to fits, excluding the e^+e^- annihilation to 3π data. The second and third data columns report on the fits performed on the same amputated \mathcal{H}_R sample set, completed with the η/η' dipion spectra under the conditions indicated in the top line of the Table ($P_X(s) = P_\eta(s) \equiv P_{\eta'}(s)$). The fair probability values can be emphasized. The last data column displays the fit results when using the A_+ variant.

one from the WASA-at-COSY Collaboration $\alpha_1 = 1.89 \pm 0.25_{stat} \pm 0.59_{syst} \pm 0.02_{th}$ [56], soon followed by $\alpha_1 = 1.96 \pm 0.27_{fit} \pm 0.02_{F\pi}$ [62]; more precise evaluations have been proposed²⁴ since (GeV⁻²) :

$$\alpha_1 = 1.32 \pm 0.08_{stat} \pm 0.10_{syst} \pm 0.02_{th} [57], \quad \alpha_1 = 1.52 \pm 0.06_{stat} [64] . \quad (40)$$

Our own evaluation – reported in Table 2 – is in good agreement ($\simeq 1\sigma$) with the KLOE/KLOE2 Collaboration result [57].

- **jj/** As far as we know, there are only two evaluations for the $P_{\eta'}(s)$ coefficients available in the literature, the former from the BESIII Collaboration [53] :

$$\text{BESIII} : \left\{ \begin{array}{l} \alpha'_1(\text{ GeV}^{-2}) = 0.992 \pm 0.039_{stat} \pm 0.067_{syst} \pm 0.163_{th} \\ \alpha'_2(\text{ GeV}^{-4}) = -0.523 \pm 0.039_{stat} \pm 0.066_{syst} \pm 0.181_{th} \end{array} \right\}, \quad (41)$$

the latter from the HHHK group [66]. Actually their Tables 2 and 3 propose slightly different pairs of values with, seemingly, a preference for the latter :

$$\text{HHHK} : \left\{ \alpha'_1 = 0.523 \pm 0.046 \text{ GeV}^{-2}, \quad \alpha'_2 = -0.138 \pm 0.046 \text{ GeV}^{-4} \right\}. \quad (42)$$

²⁴Introducing a possible a_2 exchange, Reference [64] also reports for a smaller value ($\alpha_1 = 1.42 \pm 0.06_{stat}$).

Here one is faced with a surprising pattern : While the BESIII parametrization for $P_X(s)$ is far from the favored A_- variant one reported in Table 2, it is in quite remarkable accord with the A_+ solution displayed in the last data column of Table 2; as BESIII does not deal with the intrinsic relationship between the Box and the Triangle Anomalies, their modelling is not influenced by the $\pi^0 \rightarrow \gamma\gamma$ partial width issue identified in Subsection 10.3 just above. On the other hand, the HHHK parametrization displayed in Expressions (42) is clearly at variance with both parametrizations displayed in Table 2.

As a matter of conclusion, within the BHLS₂ framework, it has been shown that the conjecture $P_{\eta'}(s) = P_\eta(s)$ is a valid statement at the (high) degree of precision permitted by the spectra from the BESIII and KLOE/KLOE2 Collaborations. Moreover, Table 1 exhibits fair fit probabilities and does not reveal any noticeable tension among the dipion spectra from KLOE/KLOE2 and BESIII on the one hand and, on the other hand, the other channels embodied within the BHLS₂ fit procedure and their data, especially the dipion spectra collected in e^+e^- annihilations²⁵.

10.5 The $T^{R2}(\eta/\eta')$ Terms in BHLS₂ : The Role of ρ^\pm Exchanges

Thanks to the breaking mechanisms [17, 18] which lead to the BHLS₂ Lagrangian, the derived η/η' decay amplitudes involve ρ^\pm exchanges as depicted in Figure 1 by the diagram classes (c1) and (c2). Relying on previous works in the HLS context which have shown that $c_3 = c_4$ is fairly well accepted by the data, this constraint is assumed; as a straightforward consequence [9, 13] all diagrams involving direct AVP couplings – all proportional to $(c_3 - c_4)$ – identically vanish and, therefore, the diagram class (c1) contributions also do. Nevertheless, the (c2) diagram class, also $\mathcal{O}(\delta)$ in breakings, survives and participates to the decay amplitudes $T_{\eta'}$ and T_η at $\mathcal{O}(\delta)$. Such contributions are not involved in the BHLS₂ pion form factor $F_\pi(s)$ expression [17]; they come naturally in the derivation of the amplitude $T(\eta/\eta')$ and are not governed by an additional *ad hoc* parameter.

Even if $\mathcal{O}(\delta)$ corrections, the $T^{R2}(\eta/\eta')$ amplitudes play a noticeable role within the BHLS₂ context :

- **i/** They are necessary in order for the full amplitudes $T(\eta/\eta') = T^{NR}(\eta/\eta') + T^{R1}(\eta/\eta') + T^{R2}(\eta/\eta')$ to coincide with their analogs directly derived from the WZW Lagrangian [50, 51] at the chiral point²⁶ $s = s_{0+} = s_{0-} = 0$.

Indeed, at the chiral point, the intensities $T^\pm(\eta/\eta')$ of the $T^{R2}(\eta/\eta')$ amplitudes defined in Sections 5 and 6 write :

$$T^{R2}(\eta) = -\frac{iec_3}{4\pi^2 f_\pi^3} \left[\epsilon - \frac{A_\pm}{2} \sin \delta_P \right] \quad \text{and} \quad T^{R2}(\eta') = -\frac{iec_3}{4\pi^2 f_\pi^3} \left[\epsilon' + \frac{A_\pm}{2} \cos \delta_P \right] \quad (43)$$

²⁵It should be reminded that the KLOE08 [32], Babar [30, 31] and SND [73] dipion spectra have been discarded because of their strong tension with the rest of the \mathcal{H}_R set of samples; one can refer to the analysis in [18] for more information.

²⁶One has previously defined $s = (p_+ + p_-)^2$, $s_{0+} = (p_+ + p_0)^2$ and $s_{0-} = (p_- + p_0)^2$.

and manifestly depend on the FKTUY parameter [10] c_3 . The condition for the amplitudes $T(\eta')$ and $T(\eta)$ to coincide with those derived from the WZW Lagrangian (see Equations (17)) is that all dependencies upon the FKTUY parameters vanish at $s = s_{0+} = s_{0-} = 0$; this condition cannot be fulfilled if dropping out (artificially) the $T^{R2}(\eta/\eta')$ terms from the full amplitude expressions $T(\eta/\eta')$.

- **ii/** To identify the effects of the $T^{R2}(\eta/\eta')$ terms, fits have been performed by discarding them in the full amplitudes and rather fit using $T(\eta/\eta') = T^{NR}(\eta/\eta') + T^{R1}(\eta/\eta')$. The fits have been performed by imposing the constraint $P_\eta(s) = P_{\eta'}(s)$ and return the results collected in the next Table.

$T^{R2}(\eta/\eta')$ (off/on)	off	on
$\chi^2_{BESIII} (N = 112)$	122	102
$\chi^2_{KLOE/KLOE2} (N = 59)$	57	55
$\chi^2_{TOTAL} (N = 1246)$	1187	1154
Probability	73.0%	90.6 %

The χ^2 values indicate that $T^{R2}(\eta)$ can be safely neglected, but also that discarding $T^{R2}(\eta')$ is not safe. The $P_X(s)$ parametrization returned by the fit is :

$$\left\{ \text{A}_-/\text{no TR2} : \alpha'_1 = 0.437 \pm 0.039 \text{ GeV}^{-2}, \quad \alpha'_2 = -0.573 \pm 0.007 \text{ GeV}^{-4} \right\}, \quad (44)$$

closer to the HHHK results [66] reminded in Expressions (42) than to those in Table 2. Therefore, it is clear from the results collected in Table 2 and the other presented ones that :

1/ The η dipion spectrum is essentially insensitive to using or discarding the T^{R2} term in its parametrization,

whereas

2/ The η' dipion spectrum parametrization is significantly degraded if its T^{R2} component is dropped out. This absence may explain the reported failure of the so-called "model-dependent" fit in [53].

As a summary, one may conclude that, once the FSI effects and the $\mathcal{O}(\delta) T^{R2}$ contribution predicted by the kinetic breaking of BHLS₂ [18] are considered, the average χ^2 per data point for the η/η' dipion spectra can be considered optimum ($\langle \chi^2 \rangle \simeq 1$). Thus, at the level of precision permitted by the presently available η [57] and η' [53] dipion spectra, additional contributions beyond those of the basic vector meson nonet – like the higher mass vector mesons [53] or the $a_2(1320)$ exchanges [64] – need not be invoked.

10.6 Dealing with the Absolute Scale of the η/η' dipion spectra

Having determined the η/η' dipion spectrum lineshapes by fitting their common FSI factor $P_X(s)$ ($X = \eta/\eta'$), it remains to derive the value of the H_X 's ($X = \eta/\eta'$) to also have their absolute magnitudes. As already noted the value of the H_X constants can be derived by introducing the accepted values [59] for the $\Gamma(\eta/\eta' \rightarrow \pi^+\pi^-\gamma)$ partial widths into the fitting procedure. This can be (and has been) done and global fits have been performed in order to get the optimum values for the $\{H_\eta, H_{\eta'}, P_X(s)\}$ triplets.

Fit Parameter	NSK+KLOE fit $P_X(s)$ only	NSK+KLOE fit $P_X(s)$ & H_X	NSK+BaBar fit $P_X(s)$ only	NSK+BaBar fit $P_X(s)$ & H_X
H_η	×	0.789 ± 0.017	×	0.797 ± 0.017
$H_{\eta'}$	×	0.671 ± 0.017	×	0.682 ± 0.015
α'_1 (GeV^{-2})	1.326 ± 0.053	1.309 ± 0.055	1.248 ± 0.058	1.241 ± 0.041
α'_2 (GeV^{-4})	-0.553 ± 0.048	-0.562 ± 0.047	-0.535 ± 0.048	-0.560 ± 0.037
$10^{10} \times a_\mu(\pi\pi)$	490.09 ± 0.89	490.15 ± 0.89	494.98 ± 0.91	494.85 ± 0.88
$(\chi^2/N)_{BESIII}$	102/112	99/112	101/112	99/112
$(\chi^2/N)_{KLOE/KLOE2}$	55/59	53/59	55/59	53/59
$(\chi^2/N)_{TOTAL}$	1154/1246	1149/1248	1346/1381	1341/1383
Fit Probability	90.6 %	92.3%	55.9%	59.4%

Table 3: Main global fit results involving the KLOE+NSK and BaBar+NSK samples collected in $e^+e^- \rightarrow \pi^+\pi^-$ annihilations. On top are displayed the parameters involved in the FSI functions (see text for details) followed by the contribution to $a_\mu(\pi\pi)$ of the $[2m_\pi, 1.0 \text{ GeV}]$ energy range. The lowest bunch provides statistical information relative to the corresponding global fits.

However, regarding the $\eta/\eta' \rightarrow \pi^+\pi^-\gamma$ decays, each of the published dipion spectra is solely given by its lineshape; concerning their normalization, they are tightly related to their partial widths. It happens that the single available "measurement" for each of these decays is the corresponding RPP piece of information [59]. In this case, as just argued, the values for H_X ($X = \eta/\eta'$) can be derived through the fitting code appropriately modified to take the partial widths into account, but also algebraically once the fit to determine the $P_X(s)$ ($X = \eta/\eta'$)

function has been performed. In this case one has, using obvious notations :

$$[\Gamma(\eta/\eta' \rightarrow \pi^+\pi^-\gamma)]_{RPP} \equiv \int \left[\frac{d\Gamma_X(s)}{d\sqrt{s}} \right]_{exp.} d\sqrt{s} = H_X^2 \int \left[\frac{d\Gamma_X(s)}{d\sqrt{s}} \right]_{BHLS_2} [P_X(s)]^2 d\sqrt{s} , \quad (45)$$

the integrals being performed over the whole energy range of the $X = \eta/\eta'$ decays and the fit values for the $\Gamma(\eta/\eta' \rightarrow \pi^+\pi^-\gamma)$ partial widths coincide with the RPP pieces of information.

Two cases have been considered regarding the specific $e^+e^- \rightarrow \pi^+\pi^-$ annihilation sample combinations involved; the first one is $\{\mathcal{H}_R + \eta/\eta'\}$ which corresponds to global fitting with the $\{\text{KLOE, NSK, BESIII, CLEO-c}\}$ combination. Correspondingly, the second case involves the $\{\text{BaBar, NSK, BESIII, CLEO-c}\}$ sample combination. The relevant fit results regarding FSI are summarized in Table 3.

The average χ^2 per point of the η and η' dipion spectra are clearly insensitive to using either of the KLOE or BaBar $e^+e^- \rightarrow \pi^+\pi^-$ annihilation data within the global fit procedure. The global fit probabilities are instead quite different and correspond to our previous BHLS₂ results [17, 18]. This insensitivity to the KLOE versus BaBaR issue is well reflected by the fit results collected in the top part of Table 3: None of the P_X and H_X parameter central values is observed to differ by more than 1σ in the various fit configurations.

Similarly, as the different $P_X(s)$ parameter values derived from fitting with the various sample combinations look statistical fluctuations, differences observed between fitting only $P_X(s)$ or the $(P_X(s)\&H_{\eta/\eta'})$ triplet look statistical fluctuations. Moreover, defining $\delta_X = H_X - 1$ and focussing, for instance, on the KLOE+NSK combination, one gets :

$$\delta_\eta = -0.211 \pm 0.017 \quad , \quad \delta_{\eta'} = -0.329 \pm 0.017 \quad (46)$$

which correspond to resp. δ and δ' as defined by Stollenwerk *et al.* [62] for which these authors derived the values $\delta = -0.22 \pm 0.04$ and $\delta' = -0.40 \pm 0.09$; these are clearly identical to our δ_η and $\delta_{\eta'}$ respectively. As a last remark, it should be noted that, once $P_X(s)$ is determined – which implies that both $\frac{d\Gamma_X(s)}{d\sqrt{s}}$ and both BHLS₂ functions are known, Equation (45) implies that both H_X are not free but are algebraically related.

11 η/η' Decays : The Muon Anomalous Magnetic Moment

The renewed interest²⁷ in the η/η' physics is intimately related to dealing with the Light-by-Light contribution to the anomalous magnetic moment (AMM) of the muon. As shown above and previously in [18], the BHLS₂ approach can address accurately several topics related with the η/η' physics and its results are supported by fair probabilities; these probabilities faithfully reflect the actual behavior of each of the data samples within the global framework as the error information provided with it is embodied without any *ad hoc* enlargement inside the fitting code.

²⁷See, for instance, [63, 78] and the references collected therein.

11.1 Accuracy of the FSI Parametrization

It has been shown above that a single FSI polynomial $P_X(s)$ allows to address simultaneously both the $\eta/\eta' \rightarrow \pi^+\pi^-\gamma$ decays within the BHLS₂ framework and that second degree is quite satisfactory. The $P_X(s)$ parametrizations derived using the A_{\pm} variants of BHLS₂ displayed in Table 2 are based on the choice of the largest set of data samples collected in almost all physics channels covering the HLS energy region (e.g. up to the $\simeq \phi$ mass region) and *consistent with each other*. It was also shown that the A_- parametrization is the best favored but, nevertheless, one found it relevant to also provide the A_+ parametrization despite its (sole real) identified failure with the π^0 lifetime (or partial width) that A_+ reconstructs at more than 5σ from its commonly accepted value [59].

Data Set	$\langle \chi_{\pi\pi}^2 \rangle$	α'_1	α'_2	Prob. (%)
$\mathcal{X}_\tau + \text{KLOE08} + \eta/\eta'$	1.57	1.294 ± 0.053	-0.379 ± 0.049	61.4%
$\mathcal{X}_\tau + \text{BaBar} + \eta/\eta'$	1.20	1.249 ± 0.076	-0.522 ± 0.069	39.6%
$\mathcal{X}_\tau + \text{NSK} + \eta/\eta'$	0.98	1.314 ± 0.054	-0.606 ± 0.052	96.6%
$\mathcal{X}_\tau + \text{KLOE} + \eta/\eta'$	0.99	1.341 ± 0.054	-0.525 ± 0.050	92.4%
$\mathcal{H}_R + \eta/\eta'$	1.07	1.326 ± 0.053	-0.553 ± 0.048	90.6%
$\mathcal{X}_\tau + \eta/\eta'$	×	1.453 ± 0.060	-0.792 ± 0.065	96.3%

Table 4: The FSI parameter values from the A_- BHLS₂ variant fit. The first column indicates which is the data set combination submitted to the global fit. $\langle \chi_{\pi\pi}^2 \rangle$ indicates the average χ^2 of the timelike $F_\pi(s)$ data points of the sample named in the first column. α'_1 and α'_2 are the coefficients of resp. the first and second degree terms of $P_X(s)$. The last data column displays the probability of the corresponding global fit.

In this Section, one aims to emphasize the reliability of the A_- parametrization by examining carefully how the $P_X(s)$ parameter values evolve while using the various dipion spectra collected in e^+e^- annihilations which are known to exhibit – sometimes severe – inconsistencies among themselves.

A possible bias in the parametrizations reported in Table 2 being the choice of the dipion data samples holds for the fits because of their mutual consistency, this issue is examined first. For this purpose, it is useful to define (or remind the definition) of some sets of data samples in order to ease the reading.

Basically, the data samples²⁰ common to the sets of data samples presently embodied within the BHLS₂ based fit procedure are the $\{(\pi^0/\eta)\gamma, K_L K_S, K^+ K^-\}$ e^+e^- annihilation channels, the dipion spectra from the τ decay provided by the ALEPH, CLEO and BELLE

Collaborations and the pion and kaon spacelike spectra from NA7[76] and Fermilab [77]; let us, for clarity, name this basic set \mathcal{X}_τ .

Regarding the available $e^+e^- \rightarrow \pi^+\pi^-$ annihilation spectra, one has distinguished four groups²⁸ (two of which being, actually, one sample "groups") : **1/** The scan data collected under the name NSK (see [16] for its content), **2/** the KLOE (\equiv KLOE10+KLOE12) [27, 28] ISR data sample group, **3/** the KLOE08 ISR sample [32] and **4/** the Babar one [30, 31]. For definiteness, the largest set of data samples found consistent with each other and referred to here and before [17, 18] as \mathcal{H}_R gathers the sets \mathcal{X}_τ , NSK and KLOE just listed. Finally, the set of dipion spectra from the $\eta/\eta' \rightarrow \pi^+\pi^-\gamma$ decays [53, 57] is referred to as η/η' .

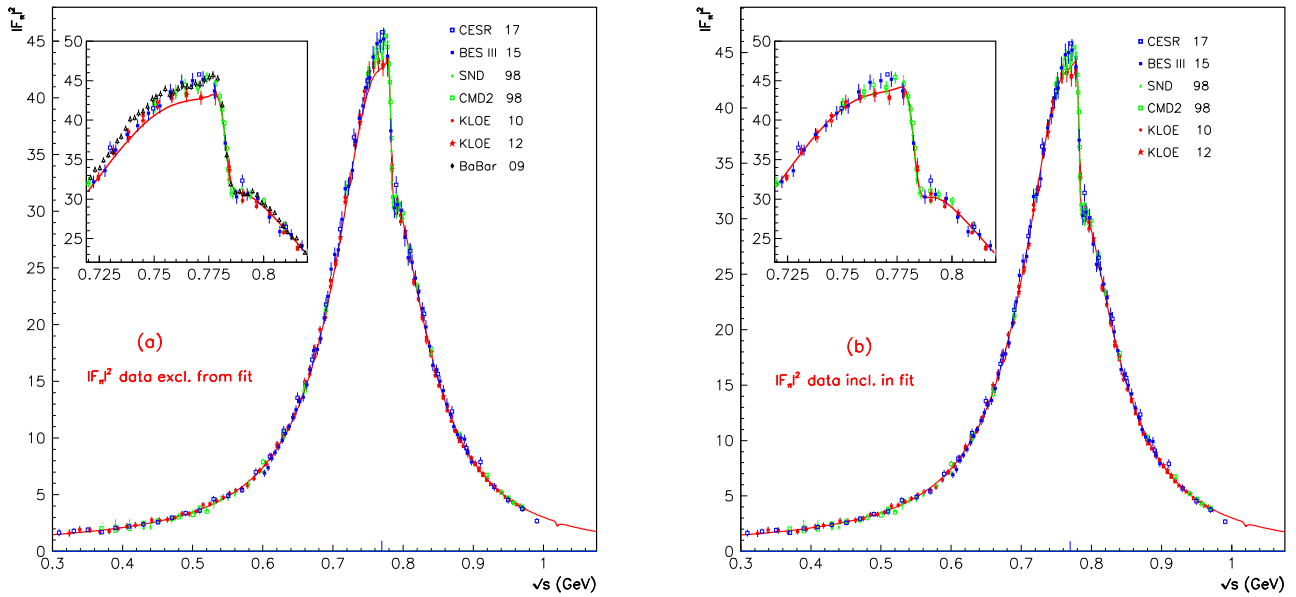


Figure 8: The curve displayed in the left-side panel (a) is the pion form factor *predicted* by fitting the data sample set $\{\mathcal{X}_\tau + \eta/\eta'\}$ and, superimposed, the *unfitted* pion form factor spectra (including those from BaBar). The right-hand side panel (b) shows the pion form factor derived from fitting the full $\{\mathcal{H}_R + \eta/\eta'\}$ data sample set which includes the KLOE and NSK pion form factors (but not the BaBar spectrum). See the text for comments.

The four top lines in Table 4 display the coefficient values of the first (α'_1) and second degree (α'_2) terms of the FSI polynomial $P_X(s)$; as indicated in its first column, the corresponding fits differ from each other only by the exact content of $e^+e^- \rightarrow \pi^+\pi^-$ annihilation spectra sample set submitted to the minimization procedure. Whatever the fit quality, reflected by its

²⁸As the more recent dipion spectra from BESIII [79, 80] and Cleo-c [20] accommodate easily any of the groups we are listing, they would not be conclusive and have been put aside for clarity; regarding the SND20 spectrum [33] deeply analyzed in our [18], we have proceeded likewise.

corresponding $\langle \chi_{\pi\pi}^2 \rangle$ value and its probability, the different values derived for α'_1 as for α'_2 are not distant by more than $(1 \div 2)\sigma$ from each other. It should also be remarked that the parameter values derived in the fit for $\{\mathcal{H}_R + \eta/\eta'\}$ – which includes the KLOE and NSK data sets together – are intermediate between those involving the KLOE and NSK sample sets separately. Therefore, the large spread of probabilities between the fits involving NSK and/or KLOE and those rather involving BaBar or KLOE08, does not produce a significant change in the determination of the common η/η' FSI function $P_X(s)$.

The last line in Table 4 displays the $P_X(s)$ coefficients returned by a fit excluding the $e^+e^- \rightarrow \pi^+\pi^-$ annihilation spectra. The linear term coefficient α'_1 is never found distant by more than $\simeq 2\sigma$ from the other corresponding values displayed in the same Table. In contrast, the curvature coefficient α'_2 exhibits a $\simeq (4 \div 5)\sigma$ departure regarding the other reported fit values. Relying on Figures 6 and 7, one expects the second degree term (α'_2) to mostly affect the $\rho^0 - \omega$ energy region. This piece of information renders interesting to compare the pion form factor *predicted* by the fit of the $\{\mathcal{X}_\tau + \eta/\eta'\}$ set²⁹ with the $e^+e^- \rightarrow \pi^+\pi^-$ annihilation data and the fit results derived when fitting the $\{\mathcal{H}_R + \eta/\eta'\}$ set. This is the purpose of Figure 8.

Comparing the curve in both panels of Figure 8, the overall agreement between both fits is fairly good, except for the magnitude at the very ρ^0 peak location which may look somewhat underestimated³⁰ by the η' dipion spectrum. Instead, the drop-off location and its intensity are fairly well predicted by the $\{\mathcal{X}_\tau + \eta/\eta'\}$ sample set.

This behavior deserves to be confirmed by new precise η' dipion spectra, complementing [53]. Indeed, within the BHLS₂ framework, the η' decay provides a mechanism 100% independent of the $e^+e^- \rightarrow \pi^+\pi^-$ annihilation process and, nevertheless, this does not prevent its prediction for $F_\pi(s)$ to exhibit a fair accord with the (fully independent) $e^+e^- \rightarrow \pi^+\pi^-$ annihilation spectra. This accord may support a possible effect beyond the Standard Model which might affect the e^+e^- annihilation channel below the ϕ meson mass to reconcile the DR approach with the FNAL measurement [2].

Regarding the FSI function $P_X(s)$, awaiting for other theoretical estimates of it, one can conclude that our favored $P_X(s)$ parametrization³¹ derived from fitting $(\mathcal{H}_R + \eta/\eta')$ provides already a reliable $P_X(s)$ and benefits from resp. a $\simeq 3\%$ and $\simeq 10\%$ precision for resp. the linear and the curvature terms.

²⁹Supplemented by the phase information between the ρ and ω propagators or by the product of branching fractions $\mathcal{B}(\omega \rightarrow e^-e^+) \times \mathcal{B}(\omega \rightarrow \pi^+\pi^-)$ available in the RPP [59].

³⁰Nevertheless, the lineshape is in good correspondance with those of the KLOE12 spectrum included in the $\{\mathcal{H}_R + \eta/\eta'\}$ sample set, but slightly smaller than the others.

³¹The $P_X(s)$ polynomial may well be interpreted as the lowest order terms of the Taylor expansion of a more complicated function which does not behave as fast as a power law; for instance, one has checked that the function $U(s) = 1 + 0.5 \log(1 + 4s)$ (*i.e.* with no free parameter) gives results identical to those derived using the second degree polynomials $P_X(s)$. Indeed the probability returned by the fit of the $\{\mathcal{H}_R + \eta/\eta'\}$ data sample set is then 91.7%, and the average χ^2 's per data point are quite favorable : For instance, 1.08 for NSK, 1.04 for KLOE, 0.92 for the BESIII η' spectrum and 0.90 for the η spectrum from KLOE/KLOE2 .

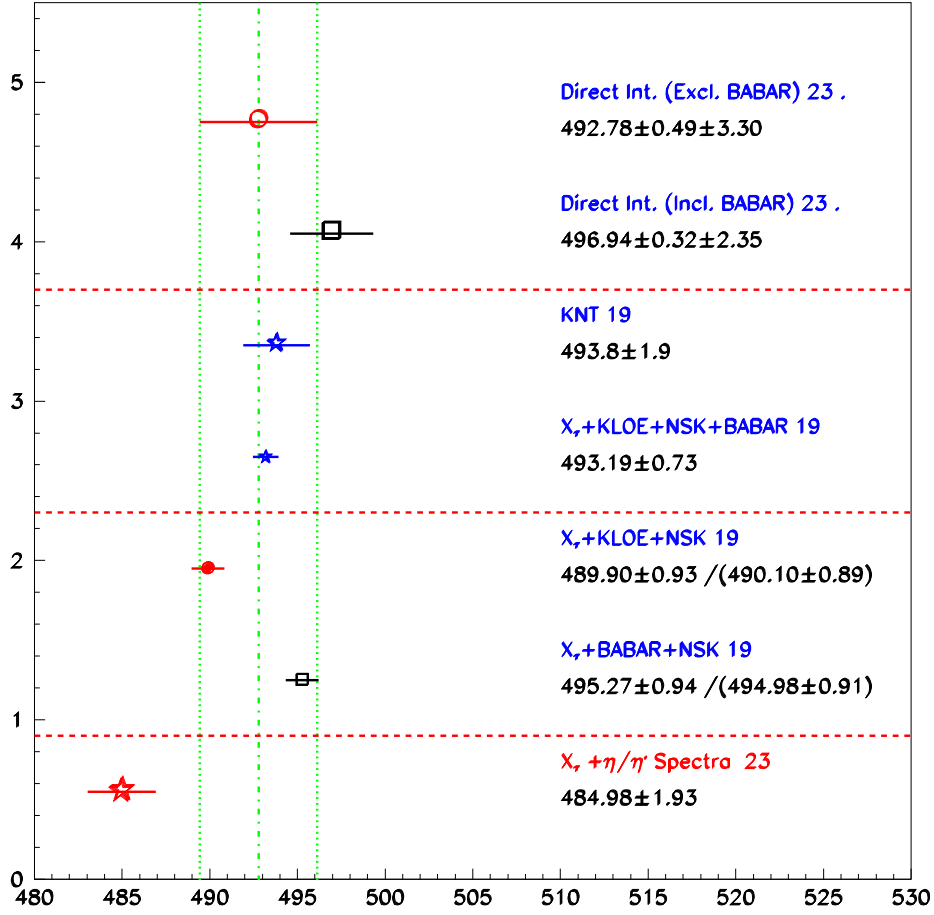


Figure 9: $a_\mu(\pi\pi, \sqrt{s} < 1.0 \text{ GeV})$ in units of 10^{-10} for various data sample combinations. The top two data points display the values derived by a direct integration of all the dipion spectra (when including BaBar, KLOE is excluded). The point tagged by KNT19 [6] is a usual (external) reference; the following point is derived using BHLS₂ with the indicated (largest) content of $e^+e^- \rightarrow \pi^+\pi^-$ spectra. The two following points show our fit results for two indicated combinations of data samples; within parentheses, one also displays the results obtained by also including the η/η' samples within the global fit procedure. The small magnitude of the BHLS₂ derived uncertainties should be noted (see text). The downmost entry in this Figure exhibits the prediction derived for $a_\mu(\pi\pi, \sqrt{s} < 1.0 \text{ GeV})$ when all annihilation to dipion data are discarded from the fit. The growth of its uncertainty reflects the drastic reduction of the statistics involved in the corresponding fit.

11.2 The η/η' Spectra and HVP Estimates

The purpose of Figure 9 is to figure out the overall picture of the estimates for $a_\mu(\pi\pi, \sqrt{s} < 1.0 \text{ GeV})$ which emerges from the present work. The top bunch data points displays the values for $a_\mu(\pi\pi, \sqrt{s} \leq 1 \text{ GeV})$ in units of 10^{-10} derived by direct integration of the dipion data taking all dipion spectra, but either excluding the Babar spectrum or excluding the KLOE spectra; the reason to proceed this way is related with inconsistencies occuring when fitting the pion form factors [18] as reported since a long time [34].

The point showing the KNT19 result [6], the usual reference [3], is followed by the evaluation derived from the BHLS₂ global fit involving $\mathcal{X}_\tau + KLOE + NSK + BABAR$ sample set which contains the same $e^+e^- \rightarrow \pi^+\pi^-$ dipion spectra³² as KNT19. The central values derived for $a_\mu(\pi\pi, \sqrt{s} \leq 1 \text{ GeV})$ are substantially identical, reflecting the fact that the normalization uncertainty treatment used to derive the KNT19 evaluation is similar to our own [81]. The BHLS₂ uncertainty is however much improved (by a factor of $\simeq 2$), as can be expected from having performed a (more constraining) global fit; indeed, within a global context, in contrast with KNT19 and others who treat the dipion spectra in a standalone mode, one benefits from also involving the τ dipion spectra and all non- $\pi\pi$ final state spectra which play as an increased statistics for all the channels involved by the underlying HLS context, in particular the $\pi\pi$ one. Therefore, comparing KNT19 and our evaluation illustrates that the BHLS₂ Lagrangian approach does not generate biases and that the difference of the central values is essentially due to the data samples chosen to derive motivatedly physical conclusions.

The top two data points of the lowest bunch substantiate numerically the amplitude of the tension between using $\mathcal{X}_\tau + KLOE + NSK$ and $\mathcal{X}_\tau + BABAR + NSK$; both agree with the direct integration results and exhibit a $\simeq 5.4 \times 10^{-10}$ distance between their evaluations of $a_\mu(\pi\pi, \sqrt{s} \leq 1 \text{ GeV})$. In both cases, the first number displayed is the evaluation derived by a standard BHLS₂ fit and is 100% consistent with the results published in [18]; the number within parentheses instead displays the result obtained when adding the η/η' data set defined above to resp. $\mathcal{X}_\tau + KLOE + NSK$ and $\mathcal{X}_\tau + BABAR + NSK$. One should note that the fit probabilities are unchanged when adding the η/η' data set and reflect fairly good fits : 88.7% \rightarrow 90.6% for $\mathcal{X}_\tau + KLOE + NSK(+\eta/\eta')$, 47.2% \rightarrow 55.9% for $\mathcal{X}_\tau + BABAR + NSK(+\eta/\eta')$. This illustrates that there is no tension between the $e^+e^- \rightarrow \pi^+\pi^-$ dipion spectra and those derived from the (η/η') decays as the probability difference between the fits involving the two data sample sets is not degraded by including the (η/η') samples.

11.3 η/η' Based Evaluations of the HVP

If, as conjectured long ago [62], an accurate enough determination of the FSI function $P_X(s)$ can be provided (by Extended ChPT [35, 36, 37], possibly), dipion spectra from the η' decay may provide a new way to estimate the dipion contribution to the muon HVP up to $\simeq 1 \text{ GeV}$. The present work has shown that phenomenology is able to provide already a FSI function $P_X(s)$ carrying a noticeable precision and, moreover, it has also been shown that a

³²It should be reminded that the corresponding fit probability is low [18] (11.4%), reflecting the KLOE–BaBar tension.

unique FSI function accomodates easily the available η and η' high precision dipion spectra simultaneously.

Indeed, within the BHLS₂ context [17, 18], the amplitudes for the $\eta/\eta' \rightarrow \pi^+\pi^-\gamma$ decays and for the $e^+e^- \rightarrow \pi^+\pi^-$ annihilation proceed from the same Lagrangian and do not call for a special treatment of their common dominant neutral ρ meson signal. Moreover, once the FSI effects are factored out, the derivation of both amplitudes from the same Lagrangian is unchanged.

On the other hand, discrepancies revealed by comparing with each other the dipion spectra collected in scan mode (NSK) and the various samples collected in ISR mode by KLOE [32, 27, 28] and Babar [30, 31] has not found a really satisfactory solution; the recent SND20 [33] – and even more, presumably, the new CMD3 [7] data – seems rather to darken the picture.

Therefore, getting high statistics dipion spectra independent of the e^+e^- annihilation mechanism, carrying different kinds of systematics, may helpfully contribute to a more satisfactory understanding of the crucial $\pi^+\pi^-$ contribution to the muon HVP.

For the time being, the limited number of high statistics η [57] and η' [53] dipion spectra allows to already derive the prediction for $a_\mu(\pi\pi, \sqrt{s} < 1.0 \text{ GeV})$ displayed in the bottom of Figure 9, namely :

$$a_\mu(\pi\pi, \sqrt{s} \leq 1 \text{ GeV}) = (484.98 \pm 1.93) \times 10^{-10} \quad (47)$$

with a 96.3 % fit probability, and is distant from its estimate based on fitting \mathcal{H}_R data sample set³³ by 2.6σ . Therefore, additional high statistics η/η' data samples can put more light on the issue, clearly located in the $\rho^0 - \omega$ invariant mass region.

12 Concluding Remarks

The present work has shown that, beside the already reported e^-e^+ annihilation spectra, some decay modes (especially the $P \rightarrow \gamma\gamma$ ones) or τ dipion spectra [17, 18], BHLS₂ can encompass the dipion spectra from the η and η' decays; however, to reach this result, one has to invoke the so-called Final State Interaction (FSI) mechanism – not a part of the HLS model – as inferred by the SHKMW group in [62].

Supplying BHLS₂ with a FSI function, one has thus obtained a fairly good simultaneous fit of the η and η' dipion spectra together with the e^+e^- annihilations into $\pi^+\pi^-/K\bar{K}/\pi^0\gamma/\eta\gamma$ final states and the $\tau^\pm \rightarrow \pi^\pm\pi^0\nu_\tau$ decay usually addressed by BHLS₂ framework in our previous [17, 18].

This proves that, once the FSI mechanism is accounted for, the BESIII η' spectrum [53] does not need more information that those already present in BHLS₂ to get a satisfactory picture; the picture is found as fair for the η spectrum reported in [57] – and, actually, even for those in [56]. The role of charged ρ meson – a natural feature of BHLS₂, [18], never considered elsewhere – has been shown to provide a fair treatment of the $\eta' \rightarrow \pi^+\pi^-\gamma$ dipion spectrum.

³³It is interesting to note that the distance between this prediction and the solution derived using NSK+KLOE is almost equal to the distance between the NSK+KLOE and NSK+BaBar solutions.

This turns out to state that most of the parameters needed to write out the relevant decay amplitudes are not free but numerically shared with the other channels embodied within the same BHLS₂ framework. This is an additional step in the proof that a unified Effective Lagrangian can fairly describe the low energy physics up to and including the ϕ mass region.

The additional parameters, needed to achieve a good description of these η/η' decay spectra are those involved by the FSI mechanism³⁴. One has first shown that the η and η' dipion spectra are well fitted with specific low degree FSI polynomials supplementing the amplitudes derived from the BHLS₂ Lagrangian. In a second step, it has been proved that, actually, a same second degree FSI polynomial $P_X(s)$ is involved in the considered η and η' decays as inferred in [62]. As already noted, the ρ^\pm exchange implied by the kinetic breaking defined in [18] is shown to enhance the global fit quality. The polynomial coefficients have been derived from our fits with fair precision and found that they remain stable when varying the fit conditions (see Table 4).

It should be noted that the picture revealed by comparing both panels of Figure 8 strikingly suggests that the traditionally used dipion spectra carry a lineshape favored by the η' dipion spectrum and that higher statistics on this can be a helpful tool in the present controversy concerning the Dispersive (DR) approaches and LQCD. Moreover, the systematics affecting the η' dipion spectrum are certainly independent of those involved in the $e^-e^+ \rightarrow \pi^+\pi^-$ annihilation. At its level of accuracy, the present η' dipion spectrum [53] rather favors the DR prediction, as shown in Figure 9; however better statistics and a finer binning in the $\rho^0 - \omega$ energy region looks mandatory for a competing estimate of the muon $a_\mu(\pi^+\pi^-, \sqrt{s} < 1.0 \text{ GeV})$. This may motivate to enlarge the available η' dipion sample by analyzing the already existing data or to collect new samples at other detectors.

Acknowledgements

We gratefully acknowledge Andrzej Kupsc, Uppsala University, for having provided the KLOE/KLOE2 and the BESIII dipion spectra; additional information on these have also been quite helpful. The CNRS/IN2P3 Computing Center (Lyon - France) is also gratefully acknowledged for having provided the computing and data-processing resources needed for this work.

Appendices

A Brief Outline of the HLS/BHLS₂ Approach

For the reader convenience, it looks worth to avoid too much cross-references and briefly collect here the various ingredients which participate to the definition and working of our symmetry broken Hidden Local Symmetry (HLS) model which are spread out into several references. The HLS model admits a non-anomalous sector [9] and, beside, an anomalous one

³⁴One may notice the parameter free FSI choice given in footnote 31 which might have to be further explored.

[10] — see also [13]. To make this approach a successful tool in its physical realm, the HLS model should undergo, symmetry breaking mechanisms. The salient features of the broken version named BHLS₂ which underly the present study can be found, reminded or defined, in³⁵ [17, 18]. As it grounds the present study, the anomalous sector of the HLS model [10, 13] is mostly discussed in the body of the text.

A.1 The Unbroken Non-Anomalous HLS Lagrangian

The non-anomalous HLS Lagrangian is a generalization of the ChPT Lagrangian [82, 83] which can be written [13] :

$$\mathcal{L}_{\text{chiral}} = \frac{f_\pi^2}{4} \text{Tr} [\partial_\mu U \partial^\mu U^\dagger] = -\frac{f_\pi^2}{4} \text{Tr} \left[\partial_\mu \xi_L \xi_L^\dagger - \partial_\mu \xi_R \xi_R^\dagger \right]^2, \quad (48)$$

where f_π ($= 92.42$ MeV) is the pion decay constant and :

$$\xi_{R/L}(x) = \exp [\pm iP(x)/f_\pi] \implies U(x) = \xi_L^\dagger(x) \xi_R(x), \quad (49)$$

when working in the so-called unitary gauge which removes a scalar field term in the definition of $\xi_{R/L}(x)$; $P(x)$ is the usual pseudoscalar (PS) field matrix. Ignoring in this reminder the weak sector [13, 17], the HLS approach turns out to replace in Equation (48) the usual derivative by the covariant derivative :

$$D_\mu \xi_{R/L} = \partial_\mu \xi_{R/L} - igV_\mu \xi_{R/L} + ie\xi_{R/L} A_\mu Q, \quad (50)$$

where A_μ is the photon field, $Q = \text{Diag}[2/3, -1/3, -1/3]$ the quark charge matrix and V_μ is the vector field matrix; the expressions for P and³⁶ V are the usual ones – fulfilling the $U(3)$ flavor symmetry – and can be found in [13, 84, 15], for example. In this way, the first HLS Lagrangian piece named \mathcal{L}_A is derived from Equation (49). However, a second piece – \mathcal{L}_V – can be defined which vanishes in the inverse substitution $D_\mu \rightarrow \partial_\mu$. The two pieces write :

$$\mathcal{L}_A = -\frac{f_\pi^2}{4} \text{Tr} \left[D_\mu \xi_L \xi_L^\dagger - D_\mu \xi_R \xi_R^\dagger \right]^2, \quad \mathcal{L}_V = -\frac{f_\pi^2}{4} \text{Tr} \left[D_\mu \xi_L \xi_L^\dagger + D_\mu \xi_R \xi_R^\dagger \right]^2. \quad (51)$$

and the full non-anomalous HLS Lagrangian writes :

$$\mathcal{L}_{\text{HLS}} = \mathcal{L}_A + a\mathcal{L}_V, \quad (52)$$

where a is a free parameter specific of the HLS approach [13]. This (unbroken) HLS Lagrangian can be found expanded in [84].

³⁵For full details the interested reader is referred to these articles, where former references can also be found.

³⁶In the V matrix the ρ , ω and ϕ fields correspond to the so-called ideal fields.

A.2 Breaking the HLS Lagrangian I : The BKY Mechanism

The first breaking mechanism for the HLS Lagrangian has been proposed in [85]; one uses a modified version of it given in [84] in order to avoid identified undesirable properties of the original proposal [86]. Originally, the BKY mechanism was intended to only break the $U(3)$ symmetry of the HLS Lagrangian; it has been extended following the lines of [87] to also cover isospin breaking effects.

Defining $L = D_\mu \xi_L \xi_L^\dagger$ and $R = D_\mu \xi_R \xi_R^\dagger$, the (modified and extended) BKY breaking is implemented in the BHLS₂ framework by modifying Equations (51) as follows :

$$\mathcal{L}_A = -\frac{f_\pi^2}{4} \text{Tr} [(L - R)X_A]^2 \quad , \quad \mathcal{L}_V = -\frac{f_\pi^2}{4} \text{Tr} [(L + R)X_V]^2 \quad , \quad (53)$$

where the constant matrices $X_{A/V}$ provide departures from the unit matrix; they have been parametrized as $X_{A/V} = \text{Diag}(q_{A/V}, y_{A/V}, z_{A/V})$. In practice, one prefers setting $q_{A/V} = 1 + (\Sigma_{A/V} + \Delta_{A/V})/2$ and $y_{A/V} = 1 + (\Sigma_{A/V} - \Delta_{A/V})/2$. As z_A and z_V are affecting the $s\bar{s}$ entries, their departure from 1 can be (and are found) large compared to $q_{A/V}$ and $y_{A/V}$ – which refer to resp. the $u\bar{u}$ and $d\bar{d}$ entries [15, 17, 18].

Within the BHLS₂ context opened in [17], it has been shown that the diagonalization of the vector meson mass term implies $\Delta_V = 0$; on the other hand, it has also been proved [17] that Σ_V is actually out of reach and can be fixed to zero without any loss of generality. Therefore the BKY breaking mechanism introduces 3 free parameters : z_A and Δ_A tightly related with the ratio f_K/f_π and z_V with the Higgs–Kibble ϕ meson mass.

A.3 Breaking the HLS Lagrangian II : The Covariant Derivative (CD) Breaking

The main ingredient in the HLS approach is the covariant derivative as displayed in Equation (50), complemented when relevant by W and Z^0 terms [13]. Thus, a relevant breaking mechanism can be chosen affecting the covariant derivative itself; this can be done by replacing Equation (50) by :

$$D_\mu \xi_{R/L} = \partial_\mu \xi_{R/L} - ig [V_\mu^I + \delta V_\mu] \xi_{R/L} + ie \xi_{R/L} A_\mu Q \quad , \quad (54)$$

where δV_μ can be chosen to break the $U(3)_V$ symmetry in a controlled way. Breaking the universality of the vector coupling g is an interesting tool; *a priori* one may think that breaking nonet symmetry (*i.e.* along the Gell–Mann matrix T^0) can be performed independently of breaking the $SU(3)_V$ symmetry (*i.e.* along the Gell–Mann matrix T^8); the diagonalization of the vector meson mass term as well as the expected values of the pion and kaon form factors at the chiral point prevent such a freedom of choice [17].

Identifying the field combinations associated with each of the canonical Gell–Mann T_a $U(3)$ matrix basis, one is led to define the following components which can participate to δV_μ

separately or together :

$$\left\{ \begin{array}{l} \delta V_\mu^0 = \frac{\xi_0}{\sqrt{2}} \left[\frac{\sqrt{2}\omega_\mu^I + \Phi_\mu^I}{3} \right] \text{Diag}[1, 1, 1], \\ \delta V_\mu^8 = \frac{\xi_8}{\sqrt{2}} \left[\frac{\omega_\mu^I - \sqrt{2}\Phi_\mu^I}{3\sqrt{2}} \right] \text{Diag}[1, 1, -2], \\ \delta V_\mu^3 = \frac{\xi_3}{\sqrt{2}} \left[\frac{\rho_I^0}{\sqrt{2}} \right] \text{Diag}[1, -1, 0], \end{array} \right. \quad (55)$$

in terms of the usual ideal field combinations; the CD breaking term is

$$\delta V_\mu = \delta V_\mu^0 + \delta V_\mu^8 + \delta V_\mu^3 .$$

The (free) breaking parameters ξ_0 , ξ_8 and ξ_3 are only requested to be real in order that δV_μ is hermitian as V_μ^I itself. Clearly, δV_μ^0 defines a breaking of the nonet symmetry down to $SU(3)_V \times U(1)_V$, δV_μ^8 rather expresses the breaking of the $SU(3)_V$ symmetry, while δV_μ^3 is related to a direct breaking of Isospin symmetry in the vector sector.

As mentioned just above, it happens that the ξ parameters introduced by Equations (55) should fulfill [17] $\xi_0 = \xi_8$ and so, that the CD breaking only involves 2 new free parameters. This means that within BHLS₂, one cannot solely break nonet symmetry which should be accompanied by a $SU(3)$ breaking of same intensity.

A.4 Breaking the HLS Lagrangian III : Dynamical Vector Meson Mixing

The unbroken HLS Lagrangian already exhibits couplings for $\rho_I/\omega_I/\phi_I \rightarrow K^+K^-/K^0\bar{K}^0$ transitions; this property is naturally transferred to all its broken versions. This implies that, at one loop order, the $\rho^0/\omega/\phi$ squared mass matrix exhibits non-diagonal entries and thus, the ideal vector fields are no longer mass eigenstates.

At one loop order, the squared mass matrix of the $\rho^0/\omega/\phi$ system can be written :

$$M^2(s) = M_0^2(s) + \delta M^2(s), \quad (56)$$

where the dependence upon the momentum squared s flowing through the vector lines is made explicit. After the *BKY* and *CD* breakings just sketched, the vector mesons masses write³⁷ :

$$\left\{ \begin{array}{l} m_{\rho^0}^2 = m^2 [1 + \Sigma_V + 2 \xi_3], \\ m_\omega^2 = m^2 \left[1 + \Sigma_V + \frac{4}{3} \xi_0 + \frac{2}{3} \xi_8 \right] = m^2 [1 + \Sigma_V + 2 \xi_0], \\ m_\Phi^2 = m^2 z_V \left[1 + \frac{2}{3} \xi_0 + \frac{4}{3} \xi_8 \right] = m^2 z_V [1 + 2 \xi_0]. \end{array} \right. \quad (57)$$

³⁷One should note that within BHLS₂ the charged and neutral ρ mesons carry different masses as $m_{\rho^\pm}^2 = m^2 (1 + \Sigma_V)$.

in terms of the various breaking parameters; Σ_V has been kept for convenience. The $M_0^2(s)$ matrix occuring in Equation (56) thus writes :

$$M_0^2(s) = \text{Diag}(m_{\rho^0}^2 + \Pi_{\pi\pi}(s), m_\omega^2, m_\phi^2) . \quad (58)$$

and is diagonal; $\Pi_{\pi\pi}(s)$ is the pion loop and includes the $\rho\pi^+\pi^-$ coupling squared.

The expression for $\delta M^2(s)$ is slightly more involved. Having defined the (ρ^0, ω, ϕ) renormalized fields, generally indexed by R (*i.e.* those which diagonalize the vector meson mass term), one can derive the $\mathcal{V}_R^i \rightarrow \mathcal{V}_R^j$ transitions ($i, j = \rho^0, \omega, \phi$). For this purpose, having defined $\Pi_\pm(s)$ and $\Pi_0(s)$, resp. the *amputated* charged and neutral kaon loops, the transition amplitudes ($i, j = \rho^0, \omega, \phi$) write :

$$\delta M_{i,j}^2(s) = g_{K^+K^-}^i g_{K^+K^-}^j \Pi_\pm(s) + g_{K^0\bar{K}^0}^i g_{K^0\bar{K}^0}^j \Pi_0(s) \quad (59)$$

where the $g_{K\bar{K}}$ coupling constants are displayed in Section 10 of [17].

The *physical* ρ^0, ω, ϕ are the eigenvectors of the full squared mass matrix $M^2(s)$; they are related to their *renormalized* partners by :

$$\begin{pmatrix} \rho_R \\ \omega_R \\ \Phi_R \end{pmatrix} = \begin{pmatrix} 1 & -\alpha(s) & \beta(s) \\ \alpha(s) & 1 & \gamma(s) \\ -\beta(s) & -\gamma(s) & 1 \end{pmatrix} \begin{pmatrix} \rho_{Phys} \\ \omega_{Phys} \\ \Phi_{Phys} \end{pmatrix} \quad (60)$$

The 3 complex angles occuring here are combinations of the $\delta M^2(s)$ matrix elements and of the eigenvalues of the full $M^2(s)$ matrix, as displayed in Subsection 10.2 of [17].

It is worth remarking that the dynamical mixing just sketched has provided the first solution [14, 15] to the long standing puzzle "e⁺e⁻ versus τ " [88, 89, 90] as it generates a s -dependent difference between the $\rho^\pm - W^\pm$ and $\rho^0 - \gamma$ transition amplitudes.

A.5 The Kinetic Breaking and the $[\pi^0, \eta, \eta']$ System

This Section mostly aims at reminding notations used in the body of the paper; these essentially deal with the pseudoscalar meson (PS) sector of the HLS model.

The full pseudoscalar meson kinetic energy term of the BHLS₂ Lagrangian [18] writes :

$$\mathcal{L}'_{kin} = \text{Tr} [\partial P_{bare} X_A \partial P_{bare} X_A] + 2 \{ \text{Tr} [X_H \partial P_{bare}] \}^2 . \quad (61)$$

where P_{bare} is the PS *bare* field matrix. The first term is already broken by the BKY mechanism applied to the \mathcal{L}_A HLS Lagrangian piece (see Equation (53) in Appendix A) and the second one expresses the so-called kinetic breaking generalizing the 'tHooft mechanism [60]. It has been shown in [18] that an appropriate choice for the X_H matrix is :

$$X_H = \lambda_0 T_0 + \lambda_3 T_3 + \lambda_8 T_8 \quad (62)$$

in terms of the canonical $U(3)$ Gell-Mann matrices ($T_0 = I/\sqrt{6}$, $\text{Tr}[T_a T_b] = \delta_{ab}/2$) with real λ_i coefficients in close correspondence with the CD breaking term δV affecting the vector sector (see Appendix A.3). This choice manifestly allows for Isospin Symmetry breaking, nonet symmetry breaking (the so-called 't Hooft term [60]) and $SU(3)$ breaking.

It is useful to introduce the vector of PS fields :

$$\mathcal{V}_{any} = (\pi_{any}^3, \eta_{any}^0, \eta_{any}^8) \quad \text{where } any = (bare, R1, R) \quad (63)$$

to clarify the component indexing.

The diagonalization of the kinetic energy Equation (61) which leads from the *bare* PS fields to their renormalized partners (hereafter indexed by R) is performed in 2 steps. The intermediate step (from *bare* to to $R1$ fields) turns out to diagonalizing $\text{Tr} [\partial P_{bare} X_A \partial P_{bare} X_A]$ and to define the W transformation matrix :

$$W = \begin{pmatrix} 1 & -\frac{\Delta_A}{\sqrt{6}} & -\frac{\Delta_A}{2\sqrt{3}} \\ -\frac{\Delta_A}{\sqrt{6}} & B & A \\ -\frac{\Delta_A}{2\sqrt{3}} & A & C \end{pmatrix} \quad (64)$$

which depends on the BKY breaking parameter Δ_A and via :

$$A = \sqrt{2} \frac{z_A - 1}{3z_A}, \quad B = \frac{2z_A + 1}{3z_A}, \quad C = \frac{z_A + 2}{3z_A} \quad (65)$$

on the other BKY breaking parameter z_A (see Appendix A.2 above).

In order to achieve the diagonalization of the (full) kinetic energy term of the BHLS₂ Lagrangian, one still has to define the linear transform which relates the intermediate $R1$ and final R renormalized PS fields (see Equation (28) in [18]). Given the (co-)vector :

$$a^t = (\lambda_3, \lambda_0 B + \lambda_8 A, \lambda_0 A + \lambda_8 C) \quad , \quad (66)$$

one can then prove [18] that Equation (61) becomes canonical (at first order in breakings) when expressed in terms of the \mathcal{V}_R fields defined by :

$$\mathcal{V}_{bare} = W \cdot \left[1 - \frac{1}{2} a \cdot a^t \right] \cdot \mathcal{V}_R \quad . \quad (67)$$

However, the \mathcal{V}_R fields are not still the PS mass eigenstates denoted by the triplet (π^0, η, η') . One expects these *physical* states to be related with the \mathcal{V}_R fields via a 3-dimensional rotation and thus 3 angles. Adopting the Leutwyler parametrization [91], one has :

$$\begin{pmatrix} \pi_R^3 \\ \eta_R^8 \\ \eta_R^0 \end{pmatrix} = \begin{pmatrix} 1 & -\epsilon & -\epsilon' \\ \epsilon \cos \theta_P + \epsilon' \sin \theta_P & \cos \theta_P & \sin \theta_P \\ -\epsilon \sin \theta_P + \epsilon' \cos \theta_P & -\sin \theta_P & \cos \theta_P \end{pmatrix} \begin{pmatrix} \pi^0 \\ \eta \\ \eta' \end{pmatrix} \quad (68)$$

to relate the R fields which diagonalize the kinetic energy to the physical (*i.e.* mass eigenstates) neutral PS fields. The three angles (ϵ , ϵ' and even θ_P) are assumed $\mathcal{O}(\delta)$ perturbations; nevertheless, for clarity, the so-called third mixing angle [61] is not treated as manifestly small.

On the other hand, the "angles" ϵ and ϵ' are related with the light quark masses and it is worth stating that they are expected likesign (see the discussion in [18]).

B Erratum : The VPP/APP interaction pieces in BHLS₂

It is worthwhile to list the VPP and APP interaction terms of the BHLS₂ Lagrangian, corrected when needed, related with the present study, *i.e.* the charged and neutral pion fields, the η and η' mesons. We have :

$$\begin{aligned}
\mathcal{L}_{\pi^-\pi^+} &= ie \left[1 - \frac{a}{2}(1 + \Sigma_V) \right] A \cdot \pi^- \overleftrightarrow{\partial} \pi^+ + \frac{ia g}{2}(1 + \Sigma_V) [1 + \xi_3] \rho_I^0 \cdot \pi^- \overleftrightarrow{\partial} \pi^+ \\
\mathcal{L}_{\pi^0\pi^\pm} &= \frac{ia g}{2}(1 + \Sigma_V) \left(1 - \frac{\lambda_3^2}{2} \right) \left[\rho^- \cdot \pi^+ \overleftrightarrow{\partial} \pi^0 - \rho^+ \cdot \pi^- \overleftrightarrow{\partial} \pi^0 \right] \\
\mathcal{L}_{\eta\pi^\pm} &= -\frac{ia g}{2} \left[\left\{ \frac{1}{2\sqrt{3}} \Delta_A + \frac{\lambda_3 \tilde{\lambda}_8}{2} \right\} \cos \theta_P - \left\{ \frac{1}{\sqrt{6}} \Delta_A + \frac{\lambda_3 \tilde{\lambda}_0}{2} \right\} \sin \theta_P + \epsilon \right] \\
&\quad [1 + \Sigma_V] \left[\rho^- \cdot \pi^+ \overleftrightarrow{\partial} \eta - \rho^+ \cdot \pi^- \overleftrightarrow{\partial} \eta \right] \\
\mathcal{L}_{\eta'\pi^\pm} &= -\frac{ia g}{2} \left[\left\{ \frac{1}{\sqrt{6}} \Delta_A + \frac{\lambda_3 \tilde{\lambda}_0}{2} \right\} \cos \theta_P + \left\{ \frac{1}{2\sqrt{3}} \Delta_A + \frac{\lambda_3 \tilde{\lambda}_8}{2} \right\} \sin \theta_P + \epsilon' \right] \\
&\quad [1 + \Sigma_V] \left[\rho^- \cdot \pi^+ \overleftrightarrow{\partial} \eta' - \rho^+ \cdot \pi^- \overleftrightarrow{\partial} \eta' \right]
\end{aligned} \tag{69}$$

The last 2 Lagrangian pieces supersede the corresponding formulae displayed in Equations (45) of [18]; they were given for completeness but unused. In the present study they should be considered.

In the expressions above, the kinetic breaking parameters occur; beside λ_3 , one also has :

$$\tilde{\lambda}_0 = \lambda_0 B + \lambda_8 A, \quad \tilde{\lambda}_8 = \lambda_0 A + \lambda_8 C \tag{70}$$

where A , B and C have also been reminded in the Appendix A.5 just above. On the other hand we have chosen, here to keep the Σ_V parameter for clarity. However in [18] it has been shown that it is out of reach and can be fixed to zero without any loss of generality.

C A_\pm Solutions : The AAP and VVP Lagrangians

It is worthwhile displaying the anomalous BHLS₂ Lagrangian pieces associated with the so-called triangle anomalies, having imposed the Kroll Conditions [58], examined in full details in [18] and briefly sketched in Section 3. Using obvious notations, these anomalous pieces

are derived from [10, 13] :

$$\left\{ \begin{array}{l} \mathcal{L}_{VVP} = -\frac{N_c g^2}{4\pi^2 f_\pi} c_3 \epsilon^{\mu\nu\alpha\beta} \text{Tr}[\partial_\mu V_\nu \partial_\alpha V_\beta P] \\ \mathcal{L}_{AAP} = -\frac{N_c e^2}{4\pi^2 f_\pi} (1 - c_4) \epsilon^{\mu\nu\alpha\beta} \partial_\mu A_\nu \partial_\alpha A_\beta \text{Tr}[Q^2 P] \\ \mathcal{L}_{AVP} = -\frac{N_c g e}{8\pi^2 f_\pi} (c_4 - c_3) \epsilon^{\mu\nu\alpha\beta} \partial_\mu A_\nu \text{Tr}[\{\partial_\alpha V_\beta, Q\} P] \end{array} \right. \quad (71)$$

The phenomenology examined so far with the broken variants of the HLS model never led to consider a non-zero $c_3 - c_4$; therefore, one assumes $c_3 = c_4$ which turns out to discard \mathcal{L}_{AVP} Lagrangian piece.

Unless otherwise stated the neutral vector fields displayed here are the so-called ideal combinations generally named ρ^I , ω^I and ϕ^I . The transformation which connects the *bare* vector fields to their *physical* partners is treated in [17] and briefly reminded in Appendix A above.

We also remind here the definition for δ_P :

$$\left\{ \begin{array}{l} \sin \delta_P = \frac{1}{\sqrt{3}} \left(\sqrt{2} \sin \theta_P - \cos \theta_P \right), \quad \cos \delta_P = \frac{1}{\sqrt{3}} \left(\sqrt{2} \cos \theta_P + \sin \theta_P \right) \end{array} \right. \quad (72)$$

and ($d_\pm \equiv \pm 1$) :

$$A_\pm = \Delta_A + d_\pm \lambda_0^2 . \quad (73)$$

used below.

C.1 The AAP Lagrangian

The AAP Lagrangian defined in the header just above where Q is the quark charge matrix and P the $U(3)$ symmetric matrix of the bare pseudoscalar fields is given for definiteness. Defining :

$$\left\{ \begin{array}{l} g_{\pi^0\gamma\gamma} = \frac{1}{6} \left\{ 1 - \frac{5}{6} A_\pm - \frac{\lambda_0^2}{3} \right\} \\ \quad - \frac{\epsilon}{18z_A} \left\{ 5z_A \sin \delta_P + \sqrt{2} \cos \delta_P \right\} - \frac{\epsilon'}{18z_A} \left\{ \sqrt{2} \sin \delta_P - 5z_A \cos \delta_P \right\}, \\ g_{\eta\gamma\gamma} = -\frac{\epsilon}{6} - \frac{\sqrt{2}}{18z_A} \cos \delta_P + \frac{1}{12} \left\{ A_\pm + \frac{5}{6} (3\lambda_0^2 - 4) \right\} \sin \delta_P \\ g_{\eta'\gamma\gamma} = -\frac{\epsilon'}{6} - \frac{\sqrt{2}}{18z_A} \sin \delta_P - \frac{1}{12} \left\{ A_\pm + \frac{5}{6} (3\lambda_0^2 - 4) \right\} \cos \delta_P \end{array} \right. \quad (74)$$

the coupling constants for the physical mesons $P_0\gamma\gamma$ ($P_0 = \pi^0, \eta, \eta'$) are given by:

$$G_{P_0\gamma\gamma} = -\frac{3\alpha_{em}}{\pi f_\pi} (1 - c_4) g_{P_0\gamma\gamma}, \quad (75)$$

and the AAP Lagrangian can also be written :

$$\mathcal{L}_{AAP_0} = G_{P_0\gamma\gamma} P_0 \epsilon^{\mu\nu\alpha\beta} \partial_\mu A_\nu \partial_\alpha A_\beta \text{ for each of } P_0 = \pi^0, \eta, \eta' . \quad (76)$$

C.2 The VVP Lagrangian

The VVP Lagrangian is given by :

$$\mathcal{L}_{VVP} = -\frac{3g^2}{4\pi^2 f_\pi} c_3 \epsilon^{\mu\nu\alpha\beta} \text{Tr} [\partial_\mu V_\nu \partial_\alpha V_\beta P] \quad , \quad C = -\frac{N_c g^2 c_3}{4\pi^2 f_\pi} , \quad (77)$$

C.2.1 The $VV\pi$ Lagrangians

The $VV\pi$ Lagrangians relevant for our phenomenology are given by :

$$\mathcal{L}_{VVP}(\pi^\pm) = \frac{C}{2} \epsilon^{\mu\nu\alpha\beta} \left\{ \left[\left(1 + \frac{2\xi_0 + \xi_8}{3} \right) \partial_\mu \omega_\nu^I + \frac{\sqrt{2}}{3} (\xi_0 - \xi_8) \partial_\mu \phi_\nu^I \right] \times [\partial_\alpha \rho_\beta^+ \pi^- + \partial_\alpha \rho_\beta^- \pi^+] \right\} \quad (78)$$

and :

$$\mathcal{L}_{VVP}(\pi^0) = \frac{C}{2} \epsilon^{\mu\nu\alpha\beta} \left\{ G_0 \partial_\mu \rho_\nu^I \partial_\alpha \omega_\beta^I + G_1 [2\partial_\mu \rho_\nu^- \partial_\alpha \rho_\beta^+ + \partial_\mu \rho_\nu^I \partial_\alpha \rho_\beta^I + \partial_\mu \omega_\nu^I \partial_\alpha \omega_\beta^I] \right. \\ \left. + G_2 \partial_\mu \phi_\nu^I \partial_\alpha \phi_\beta^I + G_3 \partial_\mu \rho_\nu^I \partial_\alpha \phi_\beta^I \right\} \pi^0 \quad (79)$$

where :

$$\left\{ \begin{array}{l} G_0 = \left[1 - \frac{\lambda_0^2}{3} + \frac{2\xi_0 + \xi_8}{3} + \xi_3 \right] \\ G_1 = -\frac{A_\pm}{4} + \frac{1}{2} [\epsilon' \cos \delta_P - \epsilon \sin \delta_P] \\ G_2 = -\frac{1}{z_A \sqrt{2}} [\epsilon' \sin \delta_P + \epsilon \cos \delta_P] \\ G_3 = \frac{\sqrt{2}}{3} (\xi_0 - \xi_8) \end{array} \right. \quad (80)$$

Actually, one imposes $\xi_0 = \xi_8$, so that, always, $G_3 = 0$.

C.2.2 The $VV\eta$ Lagrangian

The $VV\eta$ Lagrangian is given by :

$$\mathcal{L}_{VVP}(\eta) = \frac{C}{2}\epsilon^{\mu\nu\alpha\beta} \left\{ K_1\partial_\mu\rho_\nu^- \partial_\alpha\rho_\beta^+ + K_2\partial_\mu\rho_\nu^I \partial_\alpha\rho_\beta^I + K_3\partial_\mu\omega_\nu^I \partial_\alpha\omega_\beta^I + K_4\partial_\mu\phi_\nu^I \partial_\alpha\phi_\beta^I \right. \\ \left. + K_5\partial_\mu\omega_\nu^I \partial_\alpha\phi_\beta^I + K_6\partial_\mu\rho_\nu^I \partial_\alpha\omega_\beta^I \right\} \eta \quad (81)$$

Having defined³⁸ :

$$\left\{ H_2 = \frac{1}{8} [3\lambda_0^2 - 4] \quad , \quad H_3 = -\frac{\sqrt{2}}{6z_A} [(3 + 2\xi_0 + 4\xi_8)] \right\} \quad (82)$$

the $VV\eta$ couplings become :

$$\left\{ \begin{array}{l} K_1 = 2H_2 \sin \delta_P \quad , \\ K_3 = \left[H_2 - \frac{2\xi_0 + \xi_8}{3} \right] \sin \delta_P \quad , \\ K_5 = -\frac{(\xi_0 - \xi_8)}{3z_A} \left[2 \cos \delta_P + z_A \sqrt{2} \sin \delta_P \right] \quad , \end{array} \right. \quad \left\{ \begin{array}{l} K_2 = (H_2 - \xi_3) \sin \delta_P \\ K_4 = H_3 \cos \delta_P \\ K_6 = \frac{A_\pm}{2} \sin \delta_P - \epsilon \end{array} \right. \quad (83)$$

Actually, similarly to just above, the K_5 term drops out in the practical BHLS₂ context.

C.2.3 The $VV\eta'$ Lagrangian

The $VV\eta'$ Lagrangian is given by :

$$\mathcal{L}_{VVP}(\eta') = \frac{C}{2}\epsilon^{\mu\nu\alpha\beta} \left\{ K'_1\partial_\mu\rho_\nu^- \partial_\alpha\rho_\beta^+ + K'_2\partial_\mu\rho_\nu^I \partial_\alpha\rho_\beta^I + K'_3\partial_\mu\omega_\nu^I \partial_\alpha\omega_\beta^I + K'_4\partial_\mu\phi_\nu^I \partial_\alpha\phi_\beta^I \right. \\ \left. + K'_5\partial_\mu\omega_\nu^I \partial_\alpha\phi_\beta^I + K'_6\partial_\mu\rho_\nu^I \partial_\alpha\omega_\beta^I \right\} \eta' \quad (84)$$

the $VV\eta'$ couplings being :

$$\left\{ \begin{array}{l} K'_1 = -2H_2 \cos \delta_P \quad , \\ K'_3 = -\left[H_2 - \frac{2\xi_0 + \xi_8}{3} \right] \cos \delta_P \quad , \\ K'_5 = -\frac{(\xi_0 - \xi_8)}{3z_A} \left[-z_A \sqrt{2} \cos \delta_P + 2 \sin \delta_P \right] \quad , \end{array} \right. \quad \left\{ \begin{array}{l} K'_2 = -(H_2 - \xi_3) \cos \delta_P \\ K'_4 = H_3 \sin \delta_P \\ K'_6 = -\frac{A_\pm}{2} \cos \delta_P - \epsilon' \end{array} \right. \quad (85)$$

³⁸Referring to [18], the Kroll conditions turns out to fix $H_1 = 0$.

where also the K'_5 term drops out in the practical BHLS₂ context, where $\xi_0 = \xi_8$. The H_i functions occurring here have been defined in our previous paper and have been reminded in the Subsection just above – H_1 vanishes thanks to having requested the Kroll Conditions.

One should also note that the $VV\eta'$ couplings are related to the $VV\eta$ couplings and can be derived herefrom by making in the $VV\eta$ couplings :

$$\{\sin \delta_P \rightarrow -\cos \delta_P \text{ and } \cos \delta_P \rightarrow \sin \delta_P\} .$$

D A_{\pm} Solutions : The $APPP$ and $VPPP$ Lagrangians

Beside the Lagrangian pieces associated with the triangle anomalies reminded in the Appendix just above, those associated with the so-called box anomalies play an important role in the $\eta/\eta' \rightarrow \pi^+\pi^-\gamma$ decays and in the $e^+e^- \rightarrow \pi^+\pi^-\pi^0$ annihilation thoroughly considered in our [18]. We find it helpful to provide their expressions while the Kroll conditions are applied. The $APPP$ and $VPPP$ Lagrangian pieces introduce a new HLS parameter ($c_1 - c_2$) not fixed by the model and should be derived from fits.

As for the VVP interactions reminded in Appendix C, the neutral vector fields occurring in the $VPPP$ interaction Lagrangian are their ideal combinations; they should be expressed in terms of *physical* vector fields as developed in [17] in practical applications.

D.1 The $APPP$ Lagrangian

The $APPP$ Lagrangian is given by :

$$\mathcal{L}_{APPP} = D \epsilon^{\mu\nu\alpha\beta} A_\mu \text{Tr} [Q \partial_\nu P \partial_\alpha P \partial_\beta P] , \quad D = -i \frac{N_c e}{3\pi^2 f_\pi^3} \left[1 - \frac{3}{4}(c_1 - c_2 + c_4) \right] , \quad (86)$$

Regarding the phenomenology we address, the relevant $APPP$ Lagrangian piece to be considered is :

$$\mathcal{L}_{APPP}^1 = D \epsilon^{\mu\nu\alpha\beta} A_\mu \{ g_{\gamma\pi^0} \partial_\nu \pi^0 + g_{\gamma\eta} \partial_\nu \eta + g_{\gamma\eta'} \partial_\nu \eta' \} \partial_\alpha \pi^- \partial_\beta \pi^+ , \quad (87)$$

in terms of fully renormalized PS fields. Requiring the A_{\pm} Kroll conditions, these $g_{\gamma P}$ couplings can be written :

$$\begin{cases} g_{\gamma\pi^0} = -\frac{1}{4} \left[1 - \frac{A_{\pm}}{2} - \frac{\lambda_0^2}{3} - \epsilon \sin \delta_P + \epsilon' \cos \delta_P \right] \\ g_{\gamma\eta} = \left[1 - \frac{A_{\pm}}{2} - \frac{3\lambda_0^2}{4} \right] \frac{\sin \delta_P}{4} + \frac{\epsilon}{4} \\ g_{\gamma\eta'} = - \left[1 - \frac{A_{\pm}}{2} - \frac{3\lambda_0^2}{4} \right] \frac{\cos \delta_P}{4} + \frac{\epsilon'}{4} \end{cases} \quad (88)$$

keeping only the leading order terms in breakings.

D.2 The $VPPP$ Lagrangian

The $VPPP$ anomalous HLS Lagrangian is :

$$\mathcal{L}_{VPPP} = -i \frac{N_c g}{4\pi^2 f_\pi^3} (c_1 - c_2 - c_3) \epsilon^{\mu\nu\alpha\beta} \text{Tr}[V_\mu \partial_\nu P \partial_\alpha P \partial_\beta P] \quad (89)$$

where the c_i are the FKTUY parameters not fixed by the model. N_c is the number of colors fixed to 3. The V and P field matrices are the bare ones.

The relevant part of \mathcal{L}_{VPPP} within the present context is :

$$\left\{ \begin{array}{l} \mathcal{L}_{VP_0\pi^+\pi^-} = E \epsilon^{\mu\nu\alpha\beta} \{ [g_{\rho\pi}^0 \partial_\nu \pi^0 + g_{\rho\eta}^0 \partial_\nu \eta + g_{\rho\eta'}^0 \partial_\nu \eta'] \rho_\mu^I \\ + [g_{\omega\pi}^0 \partial_\nu \pi^0 + g_{\omega\eta}^0 \partial_\nu \eta + g_{\omega\eta'}^0 \partial_\nu \eta'] \omega_\mu^I + g_{\phi\pi}^0 \partial_\nu \pi^0 \phi_\mu^I \} \partial_\alpha \pi^- \partial_\beta \pi^+ \\ \text{with } E = -i \frac{3g(c_1 - c_2 - c_3)}{4\pi^2 f_\pi^3} \end{array} \right. \quad (90)$$

in terms of the *physical* pseudoscalar fields. Keeping only the A_\pm solutions and the leading order breaking terms, the couplings just defined are :

$$\left\{ \begin{array}{l} g_{\rho\pi^0}^0 = \frac{1}{4} \left[\frac{A_\pm}{2} + \epsilon \sin \delta_P - \epsilon' \cos \delta_P \right] \\ g_{\rho\eta}^0 = \frac{1}{4} \left[1 + \xi_3 - \frac{3}{4} \lambda_0^2 \right] \sin \delta_P \\ g_{\rho\eta'}^0 = -\frac{1}{4} \left[1 + \xi_3 - \frac{3}{4} \lambda_0^2 \right] \cos \delta_P \end{array} \right. \quad (91)$$

and :

$$\left\{ \begin{array}{l} g_{\omega\pi^0}^0 = -\frac{3}{4} \left[1 + \frac{2\xi_0 + \xi_8}{3} - \frac{1}{3} \lambda_0^2 \right] \\ g_{\omega\eta}^0 = \frac{3}{4} \left\{ \epsilon - \frac{A_\pm}{2} \sin \delta_P \right\} \\ g_{\omega\eta'}^0 = \frac{3}{4} \left\{ \epsilon' + \frac{A_\pm}{2} \cos \delta_P \right\} \\ g_{\phi\pi}^0 = -\frac{\sqrt{2}}{4} [\xi_0 - \xi_8] \quad , \quad g_{\phi\eta}^0 = 0, \quad g_{\phi\eta'}^0 = 0 \quad . \end{array} \right. \quad (92)$$

As pseudoscalar meson form factor values at origin imply [17] $\xi_0 = \xi_8$, one observes that no term involving ϕ^I survives at leading order in breakings.

E Brief Analysis of the BHLS₂ Parameters Values

Table 5 collects the model parameter values of the BHLS₂ Lagrangian. In order to figure out the effect of the $e^+e^- \rightarrow \pi^+\pi^-\pi^0$ annihilation data on the numerical results, its first data

column (replicated from Table 10 in [18]) displays the fit parameter values derived when they are considered, whereas the second data column provides the same information when they are excluded from the fit procedure. The third and fourth data columns report the fit results when the η/η' dipion spectra are included within the set of data samples \mathcal{H}_R amputated from the 3-pion data.

Fit Parameter	with 3π spectra	no $\eta/\eta'/3\pi$ Spectra	$P_\eta(s) \neq P_{\eta'}(s)$	$P_\eta(s) \equiv P_{\eta'}(s)$
a_{HLS}	1.766 ± 0.001	1.789 ± 0.001	1.842 ± 0.001	1.821 ± 0.001
g	6.954 ± 0.002	6.334 ± 0.001	6.236 ± 0.001	6.379 ± 0.001
$(c_3 + c_4)/2$	0.742 ± 0.003	0.756 ± 0.005	0.773 ± 0.005	0.772 ± 0.004
θ_P (degrees)	-15.59 ± 0.8	-16.471 ± 0.295	-17.614 ± 0.282	-17.433 ± 0.282
λ_0	0.285 ± 0.009	0.325 ± 0.008	0.339 ± 0.008	0.334 ± 0.008
z_A	1.406 ± 0.004	1.416 ± 0.015	1.418 ± 0.005	1.415 ± 0.005
z_V	1.420 ± 0.001	1.375 ± 0.007	1.304 ± 0.001	1.320 ± 0.001
$\Delta_A \times 10^2$	12.94 ± 4.91	12.191 ± 4.05	10.173 ± 5.39	10.249 ± 5.428
$\epsilon \times 10^2$	3.62 ± 0.30	5.383 ± 0.440	6.456 ± 0.439	6.385 ± 0.411
$\epsilon' \times 10^2$	0.17 ± 0.27	-3.623 ± 0.711	-6.809 ± 0.581	-7.021 ± 0.475
$\xi_0 \times 10^2$	-6.838 ± 0.018	1.178 ± 0.018	1.119 ± 0.013	-0.538 ± 0.014
$\xi_3 \times 10^2$	1.496 ± 0.150	6.082 ± 0.153	6.070 ± 0.136	5.609 ± 0.137
Fit Probability	83.5 %	88.6 %	89.7%	90.6%

Table 5: Fit parameter values based on the A_- BHLS₂ variant : The first data column reminds the parameter values when including the 3π spectra, the second one provides the same information when the 3π spectra are discarded from the fit procedure. The third and fourth data columns display the fit results when the η/η' spectra are included and the 3π spectra excluded.

Beside providing the parameter values themselves, the issue here is to reach an educated guess about Final State Interaction effects in the $e^+e^- \rightarrow \pi^+\pi^-\pi^0$ annihilation process : Could FSI in this channel be numerically invisible or is it absorbed effectively by the other model parameters?

First of all, the last line in Table 3 clearly shows that one always reaches fair accounts of

the spectra submitted to the BHLS₂ global fit. Regarding the parameters collected in the top bunch of the Table, one observes value differences beyond the reported fit uncertainty, however with magnitudes consistent with reasonable systematic effects.

The lower bunch of parameters looks rather confusing. Indeed, regarding ϵ , ϵ' and ξ_3 , the pieces of information derived by the three fits excluding the 3-pion data are consistent with each other and not with the first column result. The values for ξ_0 look confusing and may only indicate large systematics. Therefore, there is no obvious hint for significant FSI effects in the $e^+e^- \rightarrow \pi^+\pi^-\pi^0$ annihilation process; nevertheless, this certainly deserves devoted works [74].

References

- [1] B. Abi *et al.*, (2021), 2104.03281, Measurement of the Positive Muon Anomalous Magnetic Moment to 0.46 ppm.
- [2] Muon $g-2$, D. P. Aguillard *et al.*, 2308.06230, Measurement of the Positive Muon Anomalous Magnetic Moment to 0.20 ppm.
- [3] T. Aoyama *et al.*, Phys. Rept. **887**, 1 (2020), 2006.04822, The anomalous magnetic moment of the muon in the Standard Model.
- [4] B. L. Roberts, Chin. Phys. **C34**, 741 (2010), 1001.2898, Status of the Fermilab Muon ($g - 2$) Experiment.
- [5] M. Davier, A. Hoecker, B. Malaescu, and Z. Zhang, Eur. Phys. J. C **71**, 1515 (2011), 1010.4180, Reevaluation of the Hadronic Contributions to the Muon $g-2$ and to $\alpha(M_Z)$.
- [6] A. Keshavarzi, D. Nomura, and T. Teubner, (2018), 1802.02995, The muon $g - 2$ and $\alpha(M_Z^2)$: a new data-based analysis.
- [7] CMD-3, F. V. Ignatov *et al.*, (2023), 2302.08834, Measurement of the $e^+e^- \rightarrow \pi^+\pi^-$ cross section from threshold to 1.2 GeV with the CMD-3 detector.
- [8] R. Alemany, M. Davier, and A. Hocker, Eur. Phys. J. **C2**, 123 (1998), hep-ph/9703220, Improved determination of the hadronic contribution to the muon ($g-2$) and to $\alpha(M(Z)^{**2})$ using new data from hadronic tau decays.
- [9] M. Bando, T. Kugo, and K. Yamawaki, Phys. Rept. **164**, 217 (1988), Nonlinear Realization and Hidden Local Symmetries.
- [10] T. Fujiwara, T. Kugo, H. Terao, S. Uehara, and K. Yamawaki, Prog. Theor. Phys. **73**, 926 (1985), Nonabelian Anomaly and Vector Mesons as Dynamical Gauge Bosons of Hidden Local Symmetries.
- [11] V. V. Anashin *et al.*, Phys. Lett. **B770**, 174 (2017), 1610.02827, Measurement of R between 1.84 and 3.05 GeV at the KEDR detector.
- [12] BES, M. Ablikim *et al.*, Phys. Lett. **B677**, 239 (2009), 0903.0900, R value measurements for e^+e^- annihilation at 2.60-GeV, 3.07-GeV and 3.65-GeV.
- [13] M. Harada and K. Yamawaki, Phys. Rept. **381**, 1 (2003), hep-ph/0302103, Hidden local symmetry at loop: A new perspective of composite gauge boson and chiral phase transition.
- [14] M. Benayoun, P. David, L. DelBuono, O. Leitner, and H. B. O'Connell, Eur. Phys. J. **C55**, 199 (2008), hep-ph/0711.4482, The Dipion Mass Spectrum In e^+e^- Annihilation and tau Decay: A Dynamical (ρ^0, ω, ϕ) Mixing Approach.

- [15] M. Benayoun, P. David, L. DelBuono, and F. Jegerlehner, Eur.Phys. J. **C72**, 1848 (2012), 1106.1315, Upgraded Breaking Of The HLS Model: A Full Solution to the $\tau^- - e^+e^-$ and ϕ Decay Issues And Its Consequences On g-2 VMD Estimates.
- [16] M. Benayoun, P. David, L. DelBuono, and F. Jegerlehner, Eur.Phys. J. **C73**, 2453 (2013), 1210.7184, An Update of the HLS Estimate of the Muon g-2.
- [17] M. Benayoun, L. Delbuono, and F. Jegerlehner, Eur. Phys. J. C **80**, 81 (2020), 1903.11034, BHLS₂, a New Breaking of the HLS Model and its Phenomenology, [Erratum: Eur.Phys.J.C 80, 244 (2020)].
- [18] M. Benayoun, L. DelBuono, and F. Jegerlehner, Eur. Phys. J. C **82**, 184 (2022), 2105.13018, BHLS₂ upgrade: τ spectra, muon HVP and the [π^0 , η , η'] system.
- [19] R. R. Akhmetshin *et al.*, JETP Lett. **84**, 413 (2006), hep-ex/0610016, Measurement of the $e^+e^- \rightarrow \pi^+\pi^-$ cross section with the CMD-2 detector in the 370-MeV - 520-MeV cm energy range.
- [20] T. Xiao, S. Dobbs, A. Tomaradze, K. K. Seth, and G. Bonvicini, (2017), 1712.04530, Precision Measurement of the Hadronic Contribution to the Muon Anomalous Magnetic Moment.
- [21] ALEPH, S. Schael *et al.*, Phys. Rept. **421**, 191 (2005), hep-ex/0506072, Branching ratios and spectral functions of tau decays: Final ALEPH measurements and physics implications.
- [22] CLEO, S. Anderson *et al.*, Phys. Rev. **D61**, 112002 (2000), hep-ex/9910046, Hadronic structure in the decay $\tau^- \rightarrow \pi^- \pi^0 \nu_\tau$.
- [23] Belle, M. Fujikawa *et al.*, Phys. Rev. **D78**, 072006 (2008), 0805.3773, High-Statistics Study of the $\tau^- \rightarrow \pi^- \pi^0 \nu_\tau$ Decay.
- [24] Budapest-Marseille-Wuppertal, S. Borsanyi *et al.*, Phys. Rev. Lett. **121**, 022002 (2018), 1711.04980, Hadronic vacuum polarization contribution to the anomalous magnetic moments of leptons from first principles.
- [25] S. Borsanyi *et al.*, (2020), 2002.12347, Leading hadronic contribution to the muon magnetic moment from lattice QCD.
- [26] RBC, UKQCD, T. Blum *et al.*, Phys. Rev. Lett. **121**, 022003 (2018), 1801.07224, Calculation of the hadronic vacuum polarization contribution to the muon anomalous magnetic moment.
- [27] KLOE, F. Ambrosino *et al.*, Phys.Lett. **B700**, 102 (2011), 1006.5313, Measurement of $\sigma(e^+e^- \rightarrow \pi^+\pi^-)$ from threshold to 0.85 GeV^2 using Initial State Radiation with the KLOE detector.

- [28] KLOE Collaboration, D. Babusci *et al.*, Phys.Lett. **B720**, 336 (2013), 1212.4524, Precision measurement of $\sigma(e^+e^- \rightarrow \pi^+\pi^-\gamma)/\sigma(e^+e^- \rightarrow \mu^+\mu^-\gamma)$ and determination of the $\pi^+\pi^-$ contribution to the muon anomaly with the KLOE detector.
- [29] KLOE-2, A. Anastasi *et al.*, JHEP **03**, 173 (2018), 1711.03085, Combination of KLOE $\sigma(e^+e^- \rightarrow \pi^+\pi^-\gamma(\gamma))$ measurements and determination of $a_\mu^{\pi^+\pi^-}$ in the energy range $0.10 < s < 0.95 \text{ GeV}^2$.
- [30] BABAR, B. Aubert *et al.*, Phys. Rev. Lett. **103**, 231801 (2009), 0908.3589, Precise measurement of the $e^+e^- \rightarrow \pi^+\pi^-(\gamma)$ cross section with the Initial State Radiation method at BABAR.
- [31] BABAR Collaboration, J. Lees *et al.*, Phys.Rev. **D86**, 032013 (2012), 1205.2228, Precise Measurement of the $e^+e^- \rightarrow \pi^+\pi^-(\gamma)$ Cross Section with the Initial-State Radiation Method at BABAR.
- [32] KLOE, G. Venanzoni *et al.*, AIP Conf. Proc. **1182**, 665 (2009), 0906.4331, A precise new KLOE measurement of $|F_\pi|^2$ with ISR events and determination of $\pi\pi$ contribution to a_μ for $0.592 < M_{\pi\pi} < 0.975 \text{ GeV}$.
- [33] SND, M. Achasov *et al.*, (2020), 2004.00263, Measurement of the $e^+e^- \rightarrow \pi^+\pi^-$ process cross section with the SND detector at the VEPP-2000 collider in the energy region $0.525 < \sqrt{s} < 0.883 \text{ GeV}$.
- [34] M. BENAYOUN, Int.J.Mod.Phys.Conf.Ser. **35**, 1460416 (2014), Impact of the Recent KLOE data samples on the estimate for the muon $g - 2$.
- [35] Kaiser, R. and Leutwyler, H., Eur. Phys. J. C **17**, 623 (2000), hep-ph/0007101, Large N_c in chiral perturbation theory.
- [36] R. Kaiser and H. Leutwyler, in Adelaide 1998, Nonperturbative methods in quantum field theory , 15 (2001), hep-ph/9806336, Pseudoscalar decay constants at large N_c .
- [37] H. Leutwyler, Nucl. Phys. Proc. Suppl. **64**, 223 (1998), hep-ph/9709408, On the $1/N_c$ -expansion in chiral perturbation theory.
- [38] T. Feldmann, P. Kroll, and B. Stech, Phys.Lett. **B449**, 339 (1999), hep-ph/9812269, Mixing and decay constants of pseudoscalar mesons: The Sequel.
- [39] T. Feldmann, P. Kroll, and B. Stech, Phys. Rev. **D58**, 114006 (1998), hep-ph/9802409, Mixing and decay constants of pseudoscalar mesons.
- [40] T. Feldmann, Int. J. Mod. Phys. **A15**, 159 (2000), hep-ph/9907491, Quark structure of pseudoscalar mesons.
- [41] A. Grigorian *et al.*, Nucl. Phys. B **91**, 232 (1975), Charge Conjugation Invariance in $\eta'(958) \rightarrow \pi^+\pi^-\gamma$.

- [42] JADE, W. Bartel *et al.*, Phys. Lett. B **113**, 190 (1982), A Measurement of the Reaction $e^+e^- \rightarrow e^+e^-\eta'$ and the Radiative Width $\Gamma(\eta' \rightarrow \gamma\gamma)$ at PETRA.
- [43] CELLO, H. J. Behrend *et al.*, Phys. Lett. B **114**, 378 (1982), Determination of the Radiative Widths of the η' and A2 From Two Photon Exchange Production [Erratum: Phys.Lett.B 125, 518 (1983)].
- [44] TASSO, M. Althoff *et al.*, Phys. Lett. B **147**, 487 (1984), Measurement of the Radiative Width of the η' (958) in Two Photon Interactions.
- [45] PLUTO, C. Berger *et al.*, Phys. Lett. B **142**, 125 (1984), Measurement of Exclusive η' Production in $\gamma\gamma$ Reactions.
- [46] TPC/Two Gamma, H. Aihara *et al.*, Phys. Rev. D **35**, 2650 (1987), A study of η' formation in photon-photon collisions.
- [47] ARGUS, H. Albrecht *et al.*, Phys. Lett. **B199**, 457 (1987), Measurement of $\eta' \rightarrow \pi^+\pi^-\gamma$ in $\gamma\gamma$ collisions.
- [48] Lepton F, S. I. Bityukov *et al.*, Z. Phys. **C50**, 451 (1991), Study of the radiative decay $\eta' \rightarrow \pi^+\pi^-\gamma$.
- [49] Crystal Barrel, A. Abele *et al.*, Phys. Lett. **B402**, 195 (1997), Measurement of the decay distribution of $\eta' \rightarrow \pi^+\pi^-\gamma$ and evidence for the box anomaly.
- [50] J. Wess and B. Zumino, Phys. Lett. **B37**, 95 (1971), Consequences of anomalous Ward identities.
- [51] E. Witten, Nucl. Phys. **B223**, 422 (1983), Global Aspects of Current Algebra.
- [52] M. Benayoun, P. David, L. DelBuono, P. Leruste, and H. B. O'Connell, Eur. Phys. J. **C31**, 525 (2003), nucl-th/0306078, Anomalous η/η' decays: The triangle and box anomalies.
- [53] BESIII, M. Ablikim *et al.*, Phys. Rev. Lett. **120**, 242003 (2018), 1712.01525, Precision Study of $\eta' \rightarrow \gamma\pi^+\pi^-$ Decay Dynamics.
- [54] J. G. Layter *et al.*, Phys. Rev. **D7**, 2565 (1973), Study of dalitz-plot distributions of the decays $\eta \rightarrow \pi^+\pi^-\pi^0$ and $\eta \rightarrow \pi^+\pi^-\gamma$.
- [55] M. Gormley *et al.*, Phys. Rev. **D2**, 501 (1970), Experimental determination of the dalitz-plot distribution of the decays $\eta \rightarrow \pi^+\pi^-\pi^0$ and $\eta \rightarrow \pi^+\pi^-\gamma$, and the branching ratio $\eta \rightarrow \pi^+\pi^-\gamma$.
- [56] WASA-at-COSY, P. Adlarson *et al.*, Phys. Lett. B **707**, 243 (2012), 1107.5277, Exclusive Measurement of the $\eta \rightarrow \pi^+\pi^-\gamma$ Decay.
- [57] KLOE, D. Babusci *et al.*, Phys. Lett. B **718**, 910 (2013), 1209.4611, Measurement of $\Gamma(\eta \rightarrow \pi^+\pi^-\gamma)/\Gamma(\eta \rightarrow \pi^+\pi^-\pi^0)$ with the KLOE Detector.

- [58] P. Kroll, *Mod. Phys. Lett. A* **20**, 2667 (2005), hep-ph/0509031, Isospin symmetry breaking through $\pi^0 - \eta - \eta'$ mixing.
- [59] Particle Data Group, R. L. Workman *et al.*, *Prog.Theor.Exp.Phys.* **2022**, 083C01 (2022), Review of Particle Physics (RPP).
- [60] G. 't Hooft, *Phys. Rept.* **142**, 357 (1986), How Instantons Solve the U(1) Problem.
- [61] M. Benayoun, L. DelBuono, and H. B. O'Connell, *Eur. Phys. J. C* **17**, 593 (2000), hep-ph/9905350, VMD, the WZW Lagrangian and ChPT: The third mixing angle.
- [62] F. Stollenwerk, C. Hanhart, A. Kupsc, U. G. Meissner, and A. Wirzba, *Phys. Lett. B* **707**, 184 (2012), 1108.2419, Model-independent approach to $\eta \rightarrow \pi^+\pi^-\gamma$ and $\eta' \rightarrow \pi^+\pi^-\gamma$.
- [63] C. Hanhart, A. Kupsc, U. G. Meißner, F. Stollenwerk, and A. Wirzba, *Eur. Phys. J. C* **73**, 2668 (2013), 1307.5654, Dispersive analysis for $\eta \rightarrow \gamma\gamma^*$ [Erratum: *Eur.Phys.J.C* **75**, 242 (2015)].
- [64] B. Kubis and J. Plenzer, *Eur. Phys. J. C* **75**, 283 (2015), 1504.02588, Anomalous decay and scattering processes of the η meson.
- [65] L.-Y. Dai, X.-W. Kang, U.-G. Meißner, X.-Y. Song, and D.-L. Yao, *Phys. Rev. D* **97**, 036012 (2018), 1712.02119, Amplitude analysis of the anomalous decay $\eta' \rightarrow \pi^+\pi^-\gamma$.
- [66] S. Holz, C. Hanhart, M. Hoferichter, and B. Kubis, *Eur. Phys. J. C* **82**, 434 (2022), 2202.05846, A dispersive analysis of $\eta' \rightarrow \pi^+\pi^-\gamma$ and $\eta' \rightarrow \ell^+\ell^-\gamma$.
- [67] R. Garcia-Martin, R. Kaminski, J. R. Pelaez, J. Ruiz de Elvira, and F. J. Yndurain, *Phys. Rev. D* **83**, 074004 (2011), 1102.2183, The Pion-pion scattering amplitude. IV: Improved analysis with once subtracted Roy-like equations up to 1100 MeV.
- [68] J. Bijnens, A. Bramon, and F. Cornet, *Phys. Lett. B* **237**, 488 (1990).
- [69] B. Hyams *et al.*, *Nucl. Phys.* **B64**, 134 (1973), $\pi\pi$ Phase Shift Analysis from 600-MeV to 1900-MeV.
- [70] S. D. Protopopescu *et al.*, *Phys. Rev.* **D7**, 1279 (1973), $\pi\pi$ Partial Wave Analysis from Reactions $\pi^+p \rightarrow \pi^+\pi^-\Delta^{++}$ and $\pi^+p \rightarrow K^+K^-\Delta^{++}$ at 7.1-GeV/c.
- [71] B. Ananthanarayan, G. Colangelo, J. Gasser, and H. Leutwyler, *Phys. Rept.* **353**, 207 (2001), hep-ph/0005297, Roy equation analysis of pi pi scattering.
- [72] F. Jegerlehner and R. Szafron, *Eur. Phys. J. C* **71**, 1632 (2011), 1101.2872, $\rho^0 - \gamma$ mixing in the neutral channel pion form factor $|F_\pi|^2$ and its role in comparing e^+e^- with τ spectral functions.

- [73] SND, M. Achasov *et al.*, (2020), 2004.00263, Measurement of the $e^+e^- \rightarrow \pi^+\pi^-$ process cross section with the SND detector at the VEPP-2000 collider in the energy region $0.525 < \sqrt{s} < 0.883$ GeV.
- [74] D. Stamen, T. Isken, B. Kubis, M. Mikhasenko, and M. Niehus, (2022), 2212.11767, Analysis of rescattering effects in 3π final states.
- [75] M. Benayoun, P. David, L. DelBuono, and O. Leitner, Eur. Phys. J. **C65**, 211 (2010), 0907.4047, A Global Treatment Of VMD Physics Up To The ϕ : I. e^+e^- Annihilations, Anomalies And Vector Meson Partial Widths.
- [76] NA7, S. R. Amendolia *et al.*, Nucl. Phys. **B277**, 168 (1986), A Measurement of the Space - Like Pion Electromagnetic Form-Factor.
- [77] E. B. Dally *et al.*, Phys. Rev. Lett. **48**, 375 (1982), Elastic Scattering Measurement of the Negative Pion Radius.
- [78] L. Gan, B. Kubis, E. Passemar, and S. Tulin, Phys. Rept. **945**, 1 (2022), 2007.00664, Precision tests of fundamental physics with η and η' mesons.
- [79] BESIII, M. Ablikim *et al.*, (2015), 1507.08188, Measurement of the $e^+e^- \rightarrow \pi^+\pi^-$ Cross Section between 600 and 900 MeV Using Initial State Radiation.
- [80] BESIII, M. Ablikim *et al.*, (2020), 2009.05011, Erratum to "Measurement of the $e^+e^- \rightarrow \pi^+\pi^-$ cross section between 600 and 900 MeV using initial state radiation".
- [81] M. Benayoun, P. David, L. DelBuono, and F. Jegerlehner, Eur. Phys. J. **C75**, 613 (2015), 1507.02943, Muon $g - 2$ estimates: can one trust effective Lagrangians and global fits?
- [82] J. Gasser and H. Leutwyler, Annals Phys. **158**, 142 (1984), Chiral Perturbation Theory to One Loop.
- [83] J. Gasser and H. Leutwyler, Nucl. Phys. **B250**, 465 (1985), Chiral Perturbation Theory: Expansions in the Mass of the Strange Quark.
- [84] M. Benayoun and H. B. O'Connell, Phys. Rev. **D58**, 074006 (1998), hep-ph/9804391, SU(3) breaking and hidden local symmetry.
- [85] M. Bando, T. Kugo, and K. Yamawaki, Nucl. Phys. **B259**, 493 (1985), On the Vector Mesons as Dynamical Gauge Bosons of Hidden Local Symmetries.
- [86] A. Bramon, A. Grau, and G. Pancheri, Phys. Lett. **B345**, 263 (1995), hep-ph/9411269, Effective chiral lagrangians with an SU(3) broken vector meson sector.
- [87] M. Hashimoto, Phys. Rev. **D54**, 5611 (1996), hep-ph/9605422, Hidden local symmetry for anomalous processes with isospin/SU(3) breaking effects.

- [88] M. Davier *et al.*, Eur. Phys. J. **C66**, 127 (2010), 0906.5443, The Discrepancy Between τ and e^+e^- Spectral Functions Revisited and the Consequences for the Muon Magnetic Anomaly.
- [89] M. Davier, A. Hoecker, B. Malaescu, and Z. Zhang, Eur. Phys. J. **C71**, 1515 (2011), 1010.4180, Reevaluation of the Hadronic Contributions to the Muon g-2 and to $\alpha(MZ)$.
- [90] M. Benayoun, EPJ Web Conf. **118**, 01001 (2016), 1511.01329, The HLS approach to $(g - 2)_\mu$: A Solution to the τ versus e^+e^- Puzzle.
- [91] H. Leutwyler, Phys.Lett. **B374**, 181 (1996), hep-ph/9601236, Implications of $\eta - \eta'$ mixing for the decay $\eta \rightarrow 3\pi$.